Quantification of lightning-produced NO_x over the Pyrenees and the Ebro Valley by using different TROPOMI-NO_2 and cloud research products

Francisco J. Pérez-Invernón[1], Heidi Huntrieser[1], Thilo Erbertseder[2], Diego Loyola[3], Pieter Valks[3], Song Liu[3], Dale Allen[4], Kenneth Pickering[4], Eric Bucsela[5], Patrick Jöckel[1], Jos van Geffen[6], Henk Eskes[6], Sergio Soler[7], Francisco J. Gordillo-Vázquez[7], and Jeff Lapierre[8]

[1]Deutsches Zentrum für Luft- und Raumfahrt, Institut für Physik der Atmosphäre, Oberpfaffenhofen, Germany
[2]Deutsches Zentrum für Luft- und Raumfahrt, Deutsches Fernerkundungsdatenzentrum, Oberpfaffenhofen, Germany
[3]Deutsches Zentrum für Luft- und Raumfahrt, Methodik der Fernerkundung, Oberpfaffenhofen, Germany
[4]University of Maryland, USA
[5]SRI International, USA
[6]Royal Netherlands Meteorological Institute, Netherlands
[7]Instituto de Astrofísica de Andalucía, CSIC, Glorieta de la Astronomía s/n, Granada, Spain
[8]Earth Networks, Germantown, MD, USA

Correspondence: Francisco J. Pérez-Invernón (FranciscoJavier.Perez-Invernon@dlr.de)

Abstract. Lightning is one of the major sources of nitrogen oxides (NO_x) in the atmosphere, contributing to the tropospheric concentration of ozone and to the oxidising capacity of the atmosphere. Lightning produces between 2-8 Tg N per year globally and on average about 250 $\pm$ 150 mol NO_x per flash. In this work, we estimate the moles of NO_x produced per flash (LNO_x production efficiency) in the Pyrenees (Spain, France and Andorra) and in the Ebro Valley (Spain) by using nitrogen dioxide (NO_2) and cloud properties from the TROPOspheric Monitoring Instrument (TROPOMI) and lightning data from the Earth Networks Global Lightning Network (ENGLN) and from the EUropean Co-operation for LIghtning Detection (EUCLID). The Pyrenees is one of the areas in Europe with the highest lightning frequency and, due to its remoteness as well as experiencing very low NO_x background, enables us to better distinguish the LNO_x signal produced by recent lightning in TROPOMI NO_2 measurements. We compare the LNO_x production efficiency estimates for 8 convective systems in 2018 using two different sets of TROPOMI research products, provided by the Royal Netherlands Meteorological Institute (KNMI) and the Deutsches Zentrum für Luft- und Raumfahrt (DLR), respectively. According to our results, the mean LNO_x production efficiency in the Pyrenees and in the Ebro Valley, using a three-hour chemical lifetime, ranges between 14 and 103 mol NO_x per flash from the 8 systems. The mean LNO_x production efficiency estimates obtained using both TROPOMI products and ENGLN lightning data differ by $\sim$23%, while it differs by $\sim$35% when using EUCLID lightning data. The main sources of uncertainty when using ENGLN lightning data are the estimation of background NO_x that is not produced by lightning and the time window before the TROPOMI overpass that is used to count the total number of lightning flashes contributing to fresh-produced LNO_x. The main source of uncertainty when using EUCLID lightning data is the uncertainty in the detection efficiency of EUCLID.

1 Introduction

Lightning is one of the major sources of nitrogen oxides (NO_x = NO + NO_2) in the upper troposphere [e. g., Schumann and Huntrieser (2007) and references therein]. Lightning channels are formed by plasma reaching several thousands of Kelvin (Wallace, 1964). Such a high temperature produces dissociation of nitrogen and oxygen air molecules (Ripoll et al., 2014b, a; Kieu et al., 2021), contributing to the formation of NO_x by the Zeldovich mechanism (Zeldovich et al., 1947). Lightning-induced nitrogen oxides (LNO_x) contribute about 10% to global NO_x emissions and play an important role in determining the concentration of ozone and other chemical species in the upper troposphere as well as the oxidising capacity of the atmosphere (e.g., Labrador et al., 2005; Schumann and Huntrieser, 2007; Murray et al., 2012; Gordillo-Vázquez et al., 2019). Lightning produces between 2-8 Tg N per year globally (100-400 mol NO_x per flash) and on average about 250 mol NO_x per flash (Schumann and Huntrieser, 2007) .

Reducing the uncertainty of the NO_x production by lightning and understanding the factors that influence this production is still a challenge. Aircraft measurements have significantly contributed to determining the production of NO_x per flash, or LNO_x Production Efficiency (PE) (e.g., Huntrieser et al., 2002, 2016; Allen et al., 2021b). However, aircraft campaigns cannot provide a continuous monitoring of LNO_x and are difficult to carry out in some regions. Nadir-viewing satellite instruments such as the Ozone Monitoring Instrument (OMI), the Scanning Imaging Absorption spectroMeterfor Atmospheric CHartographY (SCIAMACHY) and the TROPOspheric Monitoring Instrument (TROPOMI) measure spectra that are used to estimate the column densities of NO_2 over thunderstorms. Several authors have used OMI NO_2 measurements to ~~estima~~ estimate the the LNO_x PE in a case-based approach or systematically over different regions (Beirle et al., 2010; Marais et al., 2018), including midlatitude regions (Bucsela et al., 2019), tropical regions (Allen et al., 2019) and the U.S. (e.g., Pickering et al., 2016; Lapierre et al., 2020; Zhang et al., 2020; Allen et al., 2021a). Satellite-based measurements can help to estimate LNO_x amounts over regions where aircraft campaigns are rare or to systematically investigate possible relationships between the characteristics of thunderstorms and LNO_x over different geographical regions (Bucsela et al., 2019). However, the opacity of thunderclouds can strongly affect the retrieval of NO_2 (Beirle et al., 2009), while convection can transport NO_x released at the surface to the upper troposphere, where it is mixed with freshly produced LNO_x. Therefore, the use of atmospheric and radiative models in combination with NO_2 measurements is needed to estimate the NO_x Production Efficiency (LNO_x PE).

The TROPOMI instrument on board the European Space Agency Sentinel-5 Precursor (S5P) satellite was launched on 13 October 2017. TROPOMI operates from a low Earth polar orbit that provides daily global measurements of several trace gases (including NO_2) and cloud properties (Veefkind et al., 2012). The horizontal resolution at nadir ~~before 6 August 2019~~ is 3.6 km $\times$ 7.2 km before 6 August 2019, while it is 3.6 km $\times$ 5.6 km thereafter. This unprecedented spatial resolution represents a unique opportunity to investigate the LNO_x PE from satellite measurements. Recently, Allen et al. (2021a) used, for the first time, TROPOMI measurements to estimate the LNO_x PE for 29 cases in the USA using lightning data from the Earth Network Global Lightning Network (ENGLN) and from the Geostationary Lightning Mapper (GLM) aboard the Geostationary Operational Environmental Satellite-16 (GOES-16). They reported 175 $\pm$ 100 and 120 $\pm$ 65 mol NO_x per flash

using ENGLN and GLM lightning data, respectively. These values are at the lower end of the globally averaged LNO_x PE of 250 ± 150 mol NO_x per flash as given by Schumann and Huntrieser (2007).

In this work, we, for the first time, quantify the amount of LNO_x over the Pyrenees and the Ebro Valley in Spain by using different TROPOMI-NO_2 and cloud research products provided by two different European research institutes, such as KNMI and DLR. The ~~geographical location of the Pyrenees and the Ebro Valley is indicated in Figure ??. The~~ Pyrenees are one of the areas in Europe with the highest lightning frequency (Molinie et al., 1999; Pineda et al., 2010; Anderson and Klugmann, 2014) and is a good place to distinguish the LNO_x signal due to its remoteness and very low NO_x background (Vinken et al., 2014). Airflows over the studied areas are influenced by the proximity of the Mediterranean Sea and the Atlantic Ocean, the high mountains of the Pyrenees, cold fronts ~~eossing~~ crossing Europe, and thermal low centered over the Iberian Peninsula (Pineda et al., 2010). In this study, we analyze 8 thunderstorms taking place in April and May 2018, the months with the highest occurrence of lightning in Spain (Pineda et al., 2010). During late spring, lightning activity in the area reaches its maximum over the mountains and is driven by solar heating (Esteban et al., 2006; Pineda et al., 2010). Therefore, we expect that during this time of the year a number of thunderstorms are active during the TROPOMI overpass ($\sim$13:30 LT). We combine two TROPOMI research products with lightning data from the ENGLN (Zhu et al., 2017; Lapierre et al., 2020) and the EUropean Co-operation for LIghtning Detection (EUCLID) systems (Schulz et al., 2016). Apart from providing new valuable estimates of LNO_x for Europe, this analysis will enable us to quantify the influence of using different lightning data sets and different TROPOMI NO_2 and cloud research products for the estimates of LNO_x PE. It is important to emphasize that the analyzed thunderstorms are not confined to the Pyrenees, but include lightning in contiguous regions where a significant boundary layer pollution can be present. Therefore, a careful analysis of the background NO_x is still needed to estimate the LNO_x over the analyzed cases.

~~Geographical location of the region of interest (Pyrenees and Ebro Valley). The map has been extracted from Blue Marble images provided by NASA (National Aeronautics and Space Administration, 2021).~~

2 Data sets and methods

2.1 TROPOMI NO_2 and cloud research products

We use TROPOMI NO_2 and cloud research products for 8 deep convective systems in the Pyrenees and contiguous regions between April and May 2018. TROPOMI is a passive imaging spectrometer with 8 spectral bands covering the ultraviolet (UV), visible (VIS), near infrared (NIR), and short-wavelength IR (SWIR) spectral regions (Veefkind et al., 2012). TROPOMI provides spectral data that is combined with different methods/algorithms to retrieve NO_2 concentrations and cloud properties (e.g., Wang et al., 2008; Loyola et al., 2018; Marais et al., 2021; Liu et al., 2021). In this work, we use two different sets of TROPOMI research products. The variables extracted from the TROPOMI products are the Slant Column Density (SCD) NO_2, the error of the SCD NO_2, the quality assurance (QA) value, the stratospheric Vertical Column Density (VCD) of NO_2, the stratospheric Air Mass Factor (AMF), the Cloud Fraction (CF) and the Optical Centroid Pressure (OCP).

The first set of TROPOMI research product is here referred to as the Royal Netherlands Meteorological Institute (KNMI) version 2.1 research product (Allen et al., 2021a) (TROP-KNMI) based on the official TROPOMI NO_2 Algorithm Theoretical Basis Document (ATBD) (van Geffen et al., 2021). This product is not automatically produced for all the TROPOMI orbits. We produce it on a case-based demand to analyze particular thunderstorms. The TROP-KNMI cloud research product is based on the Fast Retrieval Scheme for Clouds from the Oxygen A-band-S (FRESCO-S) algorithm with a Cloud as Reflecting Boundaries (CRB) model of clouds (Koelemeijer et al., 2001). In the CRB model, clouds are described as a Lambertian reflecting boundary. The separation of the contribution of the troposphere and stratosphere to the NO_2 column density for the TROP-KNMI NO_2 research product is based on a priori chemical profiles from the chemistry transport model TM5-MP ~~(Myriokefalitakis et al., 2020)~~(Williams et al., 2017; Myriokefalitakis et al., 2020). We use the version 2.1_test of this product, a modified NO_2 product that increases the data coverage over bright pixels over deep convective clouds and includes spike removal to better deal with saturation and blooming effects in the radiance spectra ~~(Ludewig et al., 2020; Allen et al., 2021a)~~ (Williams et al., 2017; Ludewig et al., 2020; Allen et al., 2021a). The reflectance value at 440 nm is reconstructed from the Differential Optical Absorption Spectroscopy (DOAS) method polynomial and the Ring correction as input to the routine that calculates the cloud (radiance) fraction in the NO_2 window. We refer to van Geffen et al. (2021); Allen et al. (2021a) for a detailed description of the TROP-KNMI NO_2 and cloud research products. Following Allen et al. (2021a), we use pixels with a quality assurance value above 0.28 (fair quality). This selection ensures that the SCD NO_2 error is less than 2 ~~petamolec cm~~$\times 10^{19}$ molec m^{-2}.

We refer to the second set of TROPOMI research product as the Deutsches Zentrum für Luft- und Raumfahrt (DLR) research product (TROP-DLR). The TROP-DLR cloud research product uses the OCRA/ROCINN algorithms for retrieving cloud properties (Loyola et al., 2018). The cloud properties provided by ROCINN uses the Clouds-As-Layers (CAL) model (Loyola et al., 2018). In the CAL model, clouds are treated as optically uniform layers using a more realistic cloud scattering model than the CRB model (Lindfors et al., 2018). We refer to Loyola et al. (2018) for a more extended description of the TROP-DLR cloud research product. The TROP-DLR NO_2 research product uses a Directionally dependent STRatospheric Estimation Algorithm from Mainz (DSTREAM) to separate the contribution of the troposphere and stratosphere to the NO_2 column density (Liu et al., 2021). This method does not require any input from atmospheric models. The STREAM method does not distinguish free tropospheric diffuse NO_2 from stratospheric NO_2. This is different in the TROP-KNMI approach, where a free tropospheric column is derived from the TM5-MP profiles. In the case of TROP-KNMI, stratospheric NO_2 retrieval does not include free tropospheric NO_2, while it does include free tropospheric NO_2 in the case of the TROP-DLR product. So, we expect the tropospheric backgrounds to be substantially higher in the TROP-KNMI product than for the TROP-DLR product. The detailed description of the TROP-DLR NO_2 research product can be found in Liu et al. (2021). In this work, we use pixels with a SCD NO_2 error lower than 2 ~~petamolec cm~~$\times 10^{19}$ molec m^{-2} to be consistent with the QA threshold defined for the TROP-KNMI product.

Pixels with deep convection are defined as pixels in which the effective cloud fraction is greater than 0.95 (Allen et al., 2021a) and the OCP value is lower than a threshold. The threshold is defined as the averaged OCP for all lightning flashes included in this study. We calculate it using OCP values for every pixels containing lightning flashes during the 5 h period

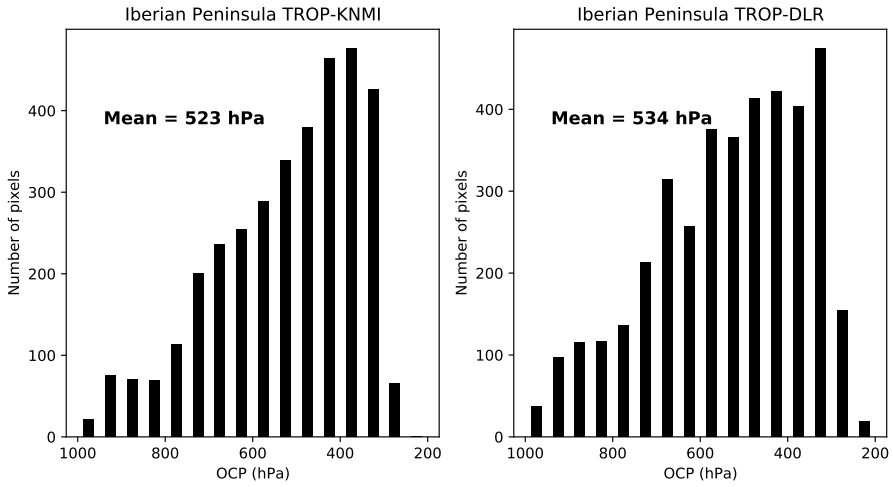

Figure 1. Distributions of OCP for pixels containing ENGLN flashes 5 hours prior to the TROPOMI overpass for the TROP-KNMI (left panel) and the TROP-DLR (right panel) products for all the studied cases.

before the TROPOMI overpass according to the TROPOMI cloud products, providing that the OCP value is not undefined. The averaged OCP for the TROP-KNMI and the TROP-DLR products are 523 hPa and 534 hPa, respectively. These pressures are slightly higher than the 500 hPa threshold employed by Pickering et al. (2016) and Allen et al. (2021a) for deep convective systems over the USA. Figure 1 shows the distributions of OCP values for TROP-KNMI and TROP-DLR using ENGLN lightning data over all the studied cases. Both distributions peak around 400 hPa, while there are more lightning flashes taking place in pixels with OCP values between 650 hPa and 500 hPa in the case of the TROP-DLR product than the TROP-KNMI product (3923 versus 3489 pixels). We have calculated the T-test for the means of the OCP distributions plotted in Figure 1, obtaining a p-value lower than 0.05. This p-value indicates that differences in the mean OCP derived from the TROP-KNMI and the TROP-DLR products are statistically significant.

2.2 Lightning measurements

We use lightning data provided by two lightning location systems, ENGLN and EUCLID, to calculate the amount of LNO_x produced per flash (or LNO_x PE).

The ENGLN is a global network composed of both broadband sensors from the Earth Networks Total Lightning Network (Liu et al., 2014) and Very Low Frequency (VLF) sensors from the World Wide Lightning Location Network (Hutchins et al., 2012) that provide the position, time of occurrence, polarity and peak current of lightning strokes. ENGLN has a Detection Efficiency (DE) of about 90% for Cloud-to-Ground (CG) strokes over the USA (Marchand et al., 2019). In this work, we use the flash product provided by ENGLN. This product is based on the flash criteria proposed by Liu and Heckman (2011), to

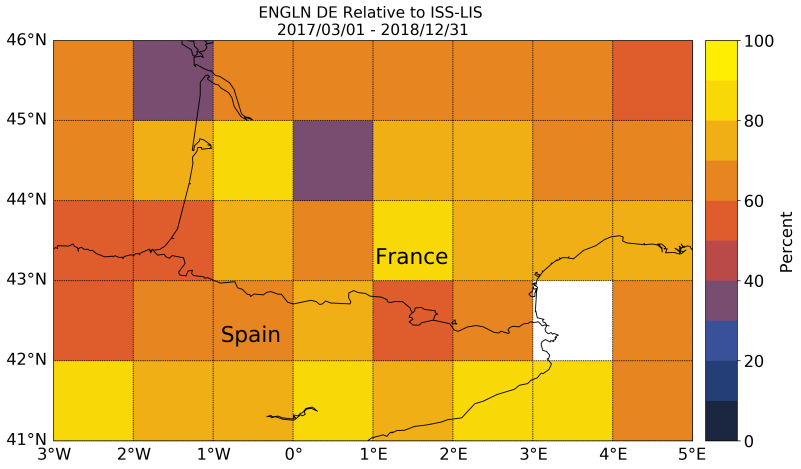

Figure 2. Spatial distribution of the ENGLN DE (in %) relative to ISS-LIS between March 2017 and December 2018 over Northern Spain, Southern France and Andorra.

cluster these strokes into flashes, in which two strokes are part of the same flash if they occur in a 0.7 s temporal window and in a 10 km spatial window.

We use lightning data from the Lightning Imaging Sensor (LIS) onboard the International Space Station (ISS) (Blakeslee et al., 2020) to estimate the DE of ENGLN over the Pyrenees. ISS-LIS detects optical emissions from lightning with a frame integration time of 1.79 ms with a spatial resolution of 4 km (Bitzer and Christian, 2015; Blakeslee et al., 2020). LIS assorts contiguous events into groups, and clusters groups into flashes with a temporal criteria of 330 ms and a spatial criteria of 5.5 km (Mach et al., 2007). ISS-LIS has a spatially uniform DE of about 60%. We compare ENGLN and ISS-LIS lightning data over the Pyrenees using the Bayesian approach proposed by Bitzer et al. (2016) with 330 ms and 25 km as the matching criteria. The Bayesian approach is more accurate than direct comparison between lightning data, as neither of the detection systems can be characterized as the truth. We show in Figure 2 the spatial distribution of the obtained ENGLN DE over the Pyrenees. The average DE in this region is 68 $\pm$ 12% based on 30 thunderstorms simultaneously detected over the are by ENGLN and ISS-LIS.

EUCLID is a European network composed of 149 lightning sensors manufactured by Vaisala Inc. and distributed over Europe (Schulz et al., 2016). Despite the high DE of EUCLID over Europe, the mean DE of EUCLID over the Pyrenees and the Ebro Valley is only about 30-60% (Poelman and Schulz) because of the low number of stations over that area and in Africa. We have selected two thunderstorms taking place between April and May 2018 over the Pyrenees and the Ebro Valley that were simultaneously detected by EUCLID and ISS-LIS. We have compared the total number of flashes reported by EUCLID and ISS-LIS in both thunderstorms, calculating a DE of 0.40 in the Pyrenees and a DE of 0.15 in the Ebro Valley. We use 27% $\pm$

12% as the DE correction for EUCLID. The significant difference between the DE of EUCLID and ENGLN over the Pyrenees represents a good opportunity to investigate the influence of Lightning Location Systems (LSS) DE on the LNO_x PE.

2.3 Meteorological and chemistry data

As we will describe in section 2.4, estimating the tropospheric background concentration of NO_x (NO_x that is not produced by lightning) is essential for the calculation of LNO_x. Although the Pyrenees is an area with relatively low background-NO_x concentration (Vinken et al., 2014), tropospheric background-NO_x can be transported from the boundary layer to the upper troposphere by convection or advected from the Ebro Valley or the city of Barcelona. Therefore, we cannot neglect the background-NO_x and have to subtract it from the VCD satellite measurements. To account for this, we use a combination of meteorological and chemical data as described below.

We use meteorological data provided by the European Centre for Medium-Range Weather Forecasts (ECMWF) ERA5-reanalysis data set. In this work, we use the 1-hourly ERA5 horizontal wind averaged between 200 hPa and 500 hPa pressure levels with a horizontal resolution of 0.25°. For each TROPOMI pixel containing lightning flashes prior to the TROPOMI overpass, we use the wind velocity and direction to estimate the advection of LNO_x. All the pixels that satisfy the deep convection constraint and that are not influenced by the spreading of LNO_x, are then considered as non-flashing pixels and employed to estimate the background-NO_x.

Alternatively, we use airborne measurements to estimate the background-NO. In particular, we use NO measurements from the In-service Aircraft for a Global Observing System (IAGOS) and from the Civil Aircraft for the Regular Investigation of the Atmosphere Based on an Instrument Container (CARIBIC) NO measurements (Brenninkmeijer et al., 2007). On 22 June, 2005, a CARIBIC flight passed over a convective system in the Pyrenees. Unfortunately, we do not have access to lightning data for that day, only cloud satellite products. However, the measured ratio NO/NO_y can be used to estimate the age of the freshly produced NO_x (Huntrieser et al., 2002). The measured ratio of NO to NO_y (about 0.1) during the passage over the convective system suggests no impact of fresh LNO_x. The measured mixing ratio of CO can be used as a proxy for upward transport of NO from the boundary layer (Huntrieser et al., 2002). Measured simultaneous increases of CO and NO on 22 June, 2005 flight suggest upward transport of polluted boundary layer air, confirming that the airplane passed across a convective system. The measured mixing ratio of NO at 12 km altitude during the passage over the convective system was 0.3 ± 0.1 ppb, in agreement with previous airborne NO measurements over convective systems without lightning in Europe during the EULINOX campaign (Huntrieser et al., 2002). We assume a NO/~~NO2~~ NO_2 ratio in the upper troposphere of 2 mol mol^{-1} (Silvern et al., 2018). Therefore, we use 0.45 ppb as an alternative to the estimation of the background-NO_x from non-flashing pixels. ~~The method we used to transform this mixing ratio of NO_x into petamolec cm^{-2} is described in more detail in Section 2.4.~~

We can estimate the VCD of NO_x using CARIBIC measurement at 12 km. We assume that the shape of the vertical profile of NO_x of the 22 June, 2005 convective system case is similar to the mean vertical profile of NO_x reported by Huntrieser et al. (2002) in Europe (Fig. 7a in (Huntrieser et al., 2002)). Using the shape of the EULINOX profile and the CARIBIC

measurement at 12 km, we can estimate the mixing ratio of NO_x between the surface and 12 km level. Finally, we can integrate the vertical profile to obtain the VCD of NO_x, resulting in 0.75 ~~petamolec cm~~ $\times 10^{19}$ molec m^{-2}.

2.4 Calculation of the LNO_x Air Mass Factor

TROPOMI provides total SCD NO_2. In the case of cloudy pixels, TROPOMI provides the SCD NO_2 over the cloud top and in the upper parts of the clouds. As we will see in section 2.5, our LNO_x PE algorithm requires the VCD LNO_x to be determined from the SCD NO_2. The ratio to convert SCD NO_2 to VCD LNO_x is called the AMF_{LNOx} and its calculation requires a priori estimations of the mean LNO_2 and LNO_x profiles over the studied region (Pickering et al., 2016) and of the absorption of the atmosphere (Beirle et al., 2009; Bucsela et al., 2013) by calculating the scattering weights for each of the 8 studied cases using the viewing geometry and the cloud properties for each pixel. It is important to note that a conversion of NO_2 SCD into NO_2 VCDs using an overall AMF followed by a conversion of VCD NO_2 into VCD NO_x using a mean NO_2 to NO_x ratio is not appropriate, as explained by Beirle et al. (2009).

We employ the ECMWF – Hamburg (ECHAM)/Modular Earth Submodel System (MESSy version 2.54.0) Atmospheric Chemistry (EMAC) model (Jöckel et al., 2016) to extract the mean LNO_2 and LNO_x profiles over the studied area by performing two simulations (with and without lightning). We perform the simulations following the Quasi Chemistry-Transport Model (QCTM) mode proposed by Deckert et al. (2011). Firstly, we perform a one year global simulation (January 1, 2018 to January 1, 2019) without lightning nudged towards ERA-Interim reanalysis meteorological fields. Secondly, we perform a second simulation with lightning for the same period using numerically identical meteorological fields as the simulation without lightning. The QCTM mode decouples the dynamics from the chemistry in order to operate the model as a chemistry-transport model, implying that small chemical perturbations do not alter the simulated meteorology by introducing noise (Deckert et al., 2011). The simulations are conducted in T42L90MA resolution, i.e. with a quadratic Gaussian grid of 2.8°×2.8° in latitude and longitude with 90 vertical levels reaching up to the 0.01 hPa pressure level and with 720 s time steps (Jöckel et al., 2016). LNO_x is calculated by using the MESSy submodel LNOX (Tost et al., 2007). Lightning is parameterized according to the updraft velocity (Grewe et al., 2001) and using a scaling factor that ensures a global lightning occurrence rate of ∼45 flashes per second (Christian et al., 2003; Cecil et al., 2014). We set the production of NO_x per flash following Price et al. (1997) and employ the C-shaped vertical profiles of LNO_x reported by Pickering et al. (1998). We use the same chemical setup and chemical mechanism as described by (Jöckel et al., 2016) for RC1 simulations.

We extract the vertical profiles of NO and NO_2 with and without lightning for May 2018 coincident with the TROPOMI overpass time to calculate the LNO_2 and LNO_x vertical profiles. We obtain that the day in May 2018 with the highest LNO_x column density is May 13, 2018. Figure 3 shows the vertical profiles obtained from the EMAC simulations. Both LNO_x and LNO_2 vertical profiles peak between 300 hPa and 250 hPa pressure levels (between ∼9 and 11 km altitude), while the vertical profiles of LNO_x and LNO_2 calculated by Pickering et al. (2016) over the Gulf of Mexico peak at about 150 hPa. The reason for this difference is that thunderstorms are taller at sub-tropical latitudes than at mid-latitudes. Non-negligible values of LNO_x and LNO_2 values between 100 and 200 hPa (Figure 3) may have been transported to the Pyrenees from tropical latitudes.

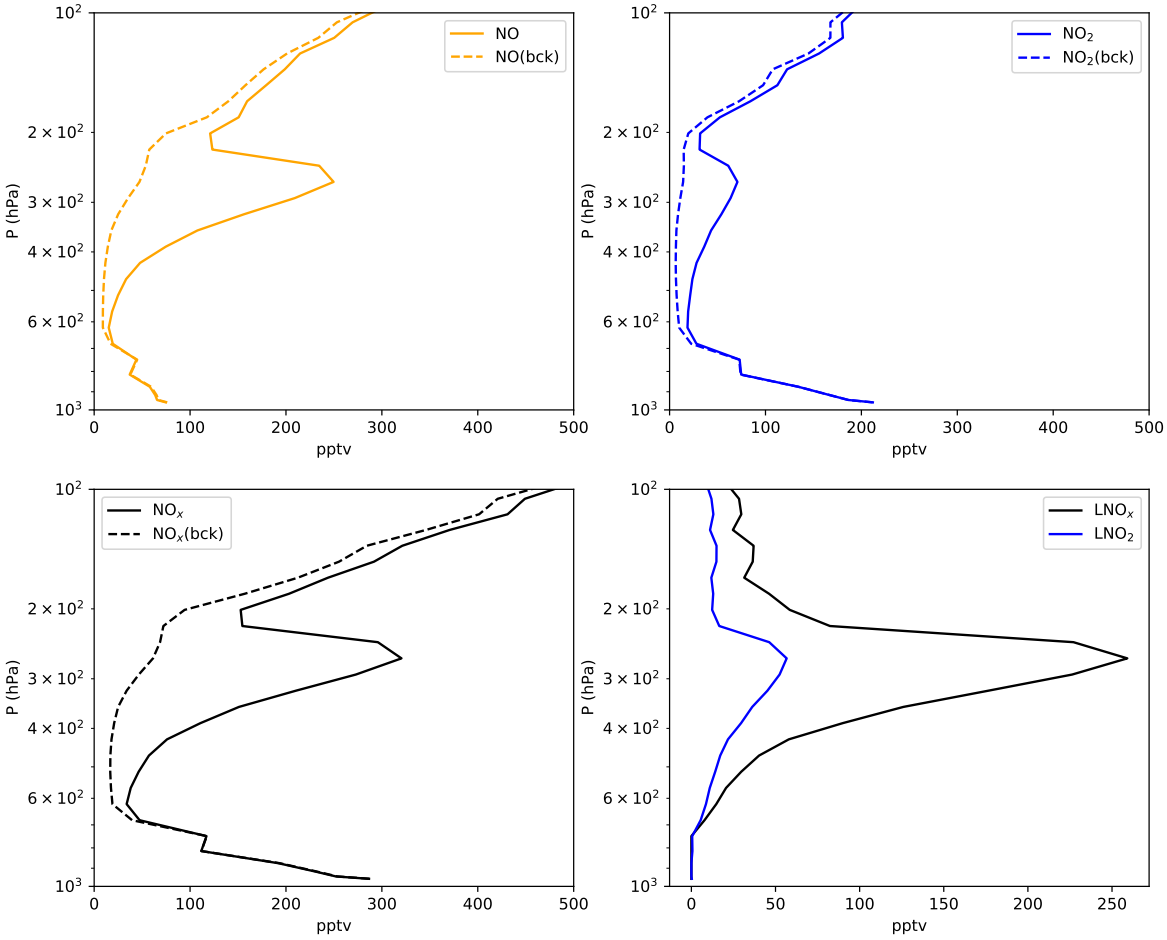

Figure 3. Vertical mixing ratio profiles of NO (upper left panel), NO_2 (upper right panel), NO_x (lower left pannel), LNO_x and LNO_2 (lower right pannel) extracted from EMAC simulations with (solid lines) and without (dashed lines) lightning (background: bck) on 13 May, 2018 at 12 h LT (close to the TROPOMI overpass).

We use the LNO_2 and LNO_x vertical profiles from the simulations to calculate the AMF_{LNOx} following Bucsela et al. (2013). We use the TOMRAD forward vector radiative transfer model (Dave, 1965) to calculate the scattering weights for each of the 8 studied cases using the viewing geometry and the cloud properties for each pixel, which depend on the TROPOMI cloud product. We obtained AMF_{LNOx} values ranging between 0.28 and 0.71.

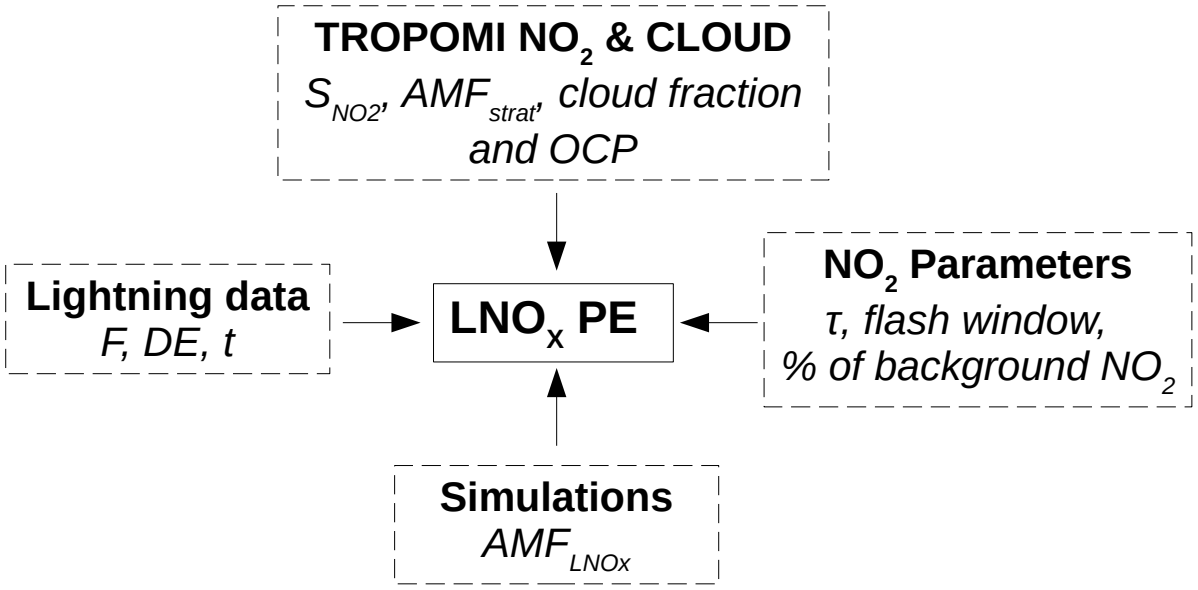

Figure 4. Overview graphic showing the variables that are included in the calculation of LNO_x PE.

2.5 Calculation of the LNO_x PE

We use the TROPOMI LNO_x PE method proposed by Allen et al. (2021a). Figure 4 shows an overview graphic indicating the variables that are included in the calculation of LNO_x PE, while Appendix 5 indicates the list of acronyms. The source of these variables are TROPOMI products, lightning data, simulations and parameters that are introduced based on literature. The LNO_x PE is calculated as

$$PE = [V_{tropLNOx} \times A] / \left[N_A \times DE^{-1} \sum_i (F \times \exp(-t_i/\tau)) \right], \quad (1)$$

where PE are the moles of NO_x produced per flash, $V_{tropLNOx}$ is the tropospheric column of NO_x produced by recent lightning (molec cm^{-2}) and that is calculated from the TROP-NO_2, A is the area (cm^{-2}) of the thunderstorm with deep convection or with undefined OCP, N_A is the Avogadro's number (molec mol^{-1}), DE is the detection efficiency of ENGLN or EUCLID, τ is the lifetime of NO_x in the near field of convection, assumed as 3 hours (Nault et al., 2017; Allen et al., 2021a)~~,~~. The lifetime is uncertain and can vary between 3 hours and 2 days [e. g., Pickering et al. (1998); Beirle et al. (2010); Nault et al. (2017) and references therein] , as it depends on the height where LNO_x is emitted and how it is transported by convection in each

particular thunderstorm. t_i is the age of individual flashes at the time of the overpass (the time since the flash occurred) and F is the total number of flashes 5 hours prior to the TROPOMI overpass of each pixel. We use a 5 h flash window because it is larger than the assumed 3 hours lifetime of NO_x in the near field of convection. Sensitivity studies using other flash windows are performed in Section 3.3.

$V_{tropLNOx}$ is calculated as

$$V_{tropLNOx} = Median(V_{tropNOx}\ \mathbf{V_{tropNOx}}) - V_{tropbck}, \quad (2)$$

where ~~$V_{tropNOx}$ is the~~ $\mathbf{V_{tropNOx}}$ is the array containing the VCD NO_x over pixels with deep convection or with undefined cloud fraction and $V_{tropbck}$ is the background-NO_x. We use the median instead of the mean of ~~$V_{tropNOx}$~~ $\mathbf{V_{tropNOx}}$ in order to remove the influence of possible outlier pixels. ~~$V_{tropNOx}$~~ $\mathbf{V_{tropNOx}}$ is defined as

$$V_{tropNOx}\ \mathbf{V_{tropNOx}} = \left[S_{NO2}\mathbf{S_{NO2}} - avg\left(V_{stratNO2} \times AMF_{strat}\ \mathbf{V_{stratNO2}} \times \mathbf{AMF_{strat}} \right) \right] / AMF_{LNOx}\mathbf{AMF_{LNOx}}, \quad (3)$$

where ~~S_{NO2} is~~ $\mathbf{S_{NO2}}$ is array containing the SCD of NO_2, ~~$V_{stratNO2}$ is the~~ $\mathbf{V_{stratNO2}}$ is the array containing the stratospheric VCD of NO_2 and ~~AMF_{strat} is the~~ $\mathbf{AMF_{strat}}$ is the array of stratospheric AMF. As previously explained by Allen et al. (2021a), values of $\mathbf{V_{stratNO2}}$ and $\mathbf{AMF_{strat}}$ are sometimes missed over pixels affected by deep convection. Therefore, using the average $\mathbf{V_{stratNO2}} \times \mathbf{AMF_{strat}}$ product increases the number of pixels available to estimate $\mathbf{V_{tropNOx}}$.

Following Allen et al. (2021a), we calculate $V_{tropbck}$ as the 30^{th} and the 10^{th} percentile of ~~$V_{tropNOx}$~~ $\mathbf{V_{tropNOx}}$ over non-flashing pixels with deep convection. These percentiles are in agreement with airborne measurements during the EULINOX campaign (Huntrieser et al., 2002). Alternatively, we calculate the background as the mean ~~$V_{tropNOx}$~~ $\mathbf{V_{tropNOx}}$ concentration averaged over three days with low lightning activity over the Pyrenees from TROPOMI data and using CARIBIC measurements in a convective system with low lightning activity over the Pyrenees (as described in section 2.3). Several events are outside the Pyrenees, with considerably higher background NO_x. Thus, the local tropospheric background estimate over the clean Pyrenees can be considered as a lower limit.

2.6 Calculation of the background-NO_x based on days with low lightning activity

Apart from calculating the background-NO_x from non-flashing pixels in a case-based approach, we have selected three cases with low lightning activity before the TROPOMI overpass to estimate the mean background-NO_x over convective systems. In particular, we have used TROPOMI measurements on 8 April, 12 April and 13 April 2018 in the region between 41°N - 45°N degrees latitude and 3°W - 5°E degrees longitude. The total number of lightning flashes 3 hour prior to the TROPOMI overpass for the three studied cases were, respectively, 149, 65 and 50. The mean $V_{tropNOx}$ during these days using the TROP-KNMI research product were 1.07 ~~petamolec cm~~ $\times\ 10^{19}$ molec m^{-2}, 1.98 ~~petamolec cm~~ $\times\ 10^{19}$ molec m^{-2} and 0.39 ~~petamolec~~

~~cm~~× 10^{19} molec m^{-2}, while the $V_{tropNOx}$ using the TROP-DLR research product were 0.37 ~~petamolec cm~~× 10^{19} molec m^{-2}, 1.00 ~~petamolec cm~~× 10^{19} molec m^{-2} and -0.5 ~~petamolec cm~~× 10^{19} molec m^{-2}. Negative values suggest that the average stratospheric column exceeding the local vertical column (eq. (3)) or the tropospheric background exceeding the signal (eq. (2)). The average background $V_{tropNOx}$ for the TROP-KNMI and the TROP-DLR research products were, respectively, 1.06 ~~petamolec cm~~× 10^{19} molec m^{-2}, and 0.37 ~~petamolec cm~~× 10^{19} molec m^{-2}. These estimates are, respectively, slightly above and below the background VCD of NO_x estimated using CARIBIC measurements (0.75 ~~petamolec cm~~× 10^{19} molec m^{-2}).

3 Results

In this section we present LNO_x estimates for 8 selected cases. We describe the TROPOMI product for the selected cases in Section 3.1. The LNO_x PE estimates are presented in Sections 3.2, while a sensitivity analysis of the results is discussed in Section 3.3.

3.1 Selected case studies

The 8 selected cases correspond to 8 thunderstorms that were active no more than 5 hours before the TROPOMI overpass on the following days: 29 April, 7 May, 12 May, 21 May, 22 May, 26 May, 28 May and 30 May 2018. Unfortunately, the TROP-DLR research product was not available for the case on 30 May ~~2018.~~ 2018 because files were missed. In addition, the thunderstorm taking place on 26 May 2018 had a significant lightning activity between 45°N and 46°N, but we do not have access to EUCLID data north of 45°N.

Figure 5 shows the ENGLN lightning data and some of the variables from the TROP-DLR product for the case 29 April 2018. Figure 6 is similar as Figure 5 but instead showing EUCLID lightning data and some of the variables from the TROP-KNMI product. Lightning activity is distributed between the Ebro Valley, the Pyrenees and the French coast.

The upper left panels of Figures 5 and 6 show the position of lightning flashes and the calculated VCD NO_x in pixels with deep convection. A comparison of the upper left of Figures 5 and 6 shows that there are more lightning flashes reported by ENGLN than by EUCLID. The upper right panels show the SCD-NO_2 for each of the used TROPOMI products, indicating that there are not significant differences between them. Areas with high lightning activity coincide with areas with high SCD-NO_2, suggesting that the LNO_x signal is detectable by TROPOMI. There are also high SCD-NO_2 values near the city of Barcelona, a highly populated area producing high emissions of NO_x. However, pixels near Barcelona do not satisfy the deep convective constrain.

The center left and right panels show the stratospheric VCD of NO_2 and the ~~stratospheric AMFof NO_2~~calculated AMF_{LNOx}, respectively. The $VCD_{stratNO2}$ from the TROP-DLR product is slightly larger than from the TROP-KNMI product, while both the stratospheric VCD of NO_2 and the stratospheric AMF of NO_2 are more homogeneous for the TROP-DLR product than for the TROP-KNMI product. The method to separate the contribution of the troposphere and stratosphere to the NO_2 column density are different for each product, which can affect the spatial distribution of the $VCD_{stratNO2}$ and the $AMF_{stratNO2}$.

The TROP-KNMI NO_2 product uses a priori chemical profiles from the chemistry transport model TM5-MP (Myriokefalitakis et al., 2020), while the TROP-DLR NO_2 product uses the DSTREAM method to separate the contribution of the troposphere and stratosphere to the NO_2 column density (Liu et al., 2021), (see section 2). Inhomogeneities in the TROP-KNMI product are due to jumps in the tropopause level associated with thunderstorms (Pan et al., 2014). The TROP-KNMI product uses the temperature of the tropopause, which may jump up and down by a few levels linked to horizontal changes in temperature gradients. The STREAM model used in the TROP-DLR product will absorb free tropospheric NO_2 into the stratosphere, while the free tropospheric background may be ~~overestimated~~ larger in the TM5-MP model which is used to estimate the stratospheric column in the TROP-KNMI product (Boersma et al., 2018). As the obtained values of AMF_{LNO_x} are different for each product because they depend on the cloud information.

Finally, the lower panels show that there are not significant differences between the cloud products, except for some pixels in which the TROP-DLR product estimates larger cloud fractions. The existence of more pixels with high cloud fractions in the TROP-DLR product ~~,~~than in the TROP-KNMI product ~~,~~can influence the total number of pixels labeled as cloud convective pixels and the calculation of the mean AMF LNO_x for each of the studied cases.

We present in Figures 7 and 8 similar plots for the case 7 May. As in the case 29 April, lightning activity is distributed between the Ebro Valley, the Pyrenees and the French coast. Areas with high lightning activity coincide with areas with high SCD-NO_2, while there are also also high SCD-NO_2 values near the city of Barcelona. We can appreciate the same differences between the TROP-KNMI and the TROP-DLR products as in the case 29 April.

Figures 9 and 10 show plots for the case 28 May 2018. In this case, lightning activity is limited to the Ebro valley and the Pyrenees. There is a profuse LNO_x signal in the SCD-NO_2 map. The stratospheric VCD of NO_2 and the stratospheric AMF of NO_2 provided by the TROP-KNMI product are more homogeneous than in the previous two cases. The rest of the cases analyzed in this study are plotted in the Supplement.

Figure 11 shows the velocity and direction of the horizontal wind averaged between the 200 hPa and 500 hPa pressure levels for the cases on 29 April, 7 May and 28 May, 2018. The average is calculated over the values provided by ERA5 in the pressure levels 200 hPa, 250 hPa, 300 hPa, 350 hPa, 400 hPa, 450 hPa and 500 hPa. On 29 April, 2018 strong southerly winds could have contributed to transport LNO_x to the north, which is in agreement with the relative position of flashes and pixels with high concentration of NO_2 as shown in Figures 6 and 5. On 7 May, 2018 northeasterly winds could have transported LNO_x to the southwest according to the location of the flashes, in agreement with Figures 7, 8. Finally, the wind velocity was weak on 28 May, 2018 and transport of lightning NO_x from the the flash positions is unlikely, in agreement with Figures 9 and 10. We have calculated the Pearson correlation coefficient (r) between the calculated VCD NO_x in convective cells and the total number of flashes reported by ENTLN in each cell averaged over all the studied cases. We have obtained r = 0.24 for TROP-DLR and r = 0.048 for TROP-KNMI. These values indicate a positive correlation between the calculated concentration of NOx and flashes that is larger for the case of TROP-DLR than for TROP-KNMI. This correlation is larger when we use the stratospheric winds to identify the cells that have been influenced by LNO_x. We have now copied each flash to the cells that are influenced by the LNO_x produced by the flash with the purpose of calculating the previous correlation coefficient by taking into account

Table 1. Results for the 8 studied cases in 2018 using the TROP-KNMI research product.

Data	Region	F ENGLN /EUCLID (N flashes)	Mean OCP (hPa)	Median $V_{tropNOx}$ ($\times 10^{19}$ molec m^{-2})	Mean $V_{stratNO2} \times AMF_{strat}$ ($\times 10^{19}$ molec m^{-2})	Mean AMF_{LNOx}	$V_{tropbck}$ 10^{th}/30^{th} ($\times 10^{19}$ molec m^{-2})	PE (ENGLN) 30^{th} / 10^{th} mol NO$_x$/ f	PE (EUCLID) 30^{th} / 10^{th} mol NO$_x$/ f
29 April	40N-45N/3W-4E	4591 / 982	628	3.8	7.5	0.72	2.7 / 3.1	22 / 42	34 / 72
7 May	41N-44N/2W-4E	5356 / 1044	346	3.4	6.9	0.36	1.3 / 2.0	30 / 47	81 / 124
12 May	40N-45N/2W-2E	1434 / 175	629	2.6	6.7	0.46	1.7 / 2.4	5 / 19	35 / 78
21 May	42N-43.8N/2W-4E	5263 / 1015	473	2.3	7.8	0.44	1.0 / 1.4	17 / 25	34 / 52
22 May	41N-43N/1W-4E	2318 / 515	530	2.6	7.8	0.46	1.6 / 1.8	19 / 26	32 / 46
26 May	41N-46N/4W-2E	25158 / 4821	593	6.4	7.2	0.34	2.8 / 3.4	86 / 103	42 / 54
28 May	41N-43N/2W-4E	7556 / 1568	494	5.2	5.7	0.45	3.5 / 3.9	52 / 72	99 / 139
30 May	41N-45N/2W-4E	9782 / 5754	502	1.8	8.9	0.80	-0.01 / 0.8	65 / 115	83 / 102
Mean $\pm$ σ			527	3.5	7.3	0.50	1.8 / 2.3	47 $\pm$ 33	69 $\pm$ 34

the transport of LNO$_x$. We have now obtained r = 0.28 for TROP-DLR and r = 0.055 for TROP-KNMI. The received larger correlation coefficients indicate that accounting for the transport of LNO$_x$ can improve the estimation of LNO$_x$ PE.

3.2 LNO$_x$ PE estimates

In this section, we present the LNO$_x$ PE estimates for the selected cases using two different methods to estimate the background-NO$_x$. The first method (subsection 3.2.1) is exclusively based on case by case TROPOMI measurements, as it uses non-flashing pixels with deep convection to estimate the background-NO$_x$. The second method (subsection 3.2.2) uses fixed values for the background-NO$_x$ from measurements over days with low lightning activity.

3.2.1 LNO$_x$ PE estimates using non-flashing pixels to estimate the background-NO$_x$

In this section, we present the LNO$_x$ PE estimates for the selected cases by using the 30^{th} and the 10^{th} percentile of $V_{tropNOx}$ over non-flashing pixels with deep convection as background-NO$_x$ estimations. Table 1 shows the results for 8 cases in the Pyrenees using the described method and the TROP-KNMI research product, while Table 2 shows the results using the TROP-DLR research product. Here we have used a 5 h time window before the TROPOMI overpass and a chemical lifetime of NO$_x$ (τ) of 3 h for all the cases shown in these tables. We have chosen these values for the flash window and τ as reference values to show the LNO$_x$ estimates in Table 1. However, later in Section 3.3, we perform a sensitivity analysis using different values for flash window and τ. The obtained case-based averages age of individual flashes range between 0.9 hours for 7 May case and 2.3 hours for 26 May case.

Columns 1 and 2 show the date and thunderstorm region of each studied case and some mean values, respectively. Column 3 shows the total number of lightning flashes reported by ENGLN/EUCLID 5 h before the TROPOMI overpass without application of a DE. The total number of flashes reported by ENGLN is always larger than reported by EUCLID. Minor differences in the total number of flashes between both TROPOMI products (compare Tables 1 and 2) are due to minor differences in the product grids.

Table 2. Results for the 7 studied cases in 2018 using the TROP-DLR research product.

Data	Region	F ENGLN /EUCLID (N flashes)	Mean OCP (hPa)	Median $V_{tropNOx}$ ($\times 10^{19}$ molec m^{-2})	Mean $V_{stratNO2} \times AMF_{strat}$ ($\times 10^{19}$ molec m^{-2})	Mean AMF_{LNOx}	$V_{tropbck}$ 10^{th}/30^{th} ($\times 10^{19}$ molec m^{-2})	PE (ENGLN) 30^{th} / 10^{th} mol NO$_x$/ f	PE (EUCLID) 30^{th} / 10^{th} mol NO$_x$/ f
29 April	40N-45N/3W-4E	4583 / 981	604	1.5	8.9	0.72	0.5 / 1.0	70 / 145	23 / 85
7 May	41N-44N/2W-4E	5241 / 1041	339	0.27	8.1	0.46	-0.8 / -0.3	22 / 43	42 / 96
12 May	40N-45N/2W-2E	1409 / 171	573	0.89	8.0	0.59	-0.8 / -0.3	40 / 78	40 / 62
21 May	42N-43.8N/2W-4E	5243 / 1012	440	0.89	8.4	0.54	0.05 / 0.5	38 / 62	37 / 47
22 May	41N-43N/1W-4E	2308 / 513	481	1.8	8.2	0.51	0.15 / 0.8	64 / 102	69 / 113
26 May	41N-46N/4W-2E	25233 / 4532	552	1.1	8.9	0.47	-0.28 / 0.3	46 / 78	13 / 37
28 May	41N-43N/2W-4E	7543 / 1563	451	1.0	8.0	0.52	-0.32 / 0.3	49 / 87	56 / 92
Mean $\pm \sigma$			491	0.96	8.3	0.54	-0.2 / 1.5	58 $\pm$ 33	51 $\pm$ 25

Column 4 shows the OCP averaged for all lightning flashes reported by ENGLN. Significant differences are obtained between the cases. As lower limit, we obtain 339 hPa from the TROP-DLR research product for 7 May case, while we obtain an upper limit of 629 hPa from the TROP-KNMI research product for the 12 May case. The mean OCP values for the TROP-KNMI and the TROP-DLR products are 527 hPa and 491 hPa, respectively. These values do not coincide with mean OCP values showed in Fig. 1 because they correspond to the mean OCP per lightning flash instead of to the mean OCP value per pixel. As a consequence, the mean OCP values showed in Column 4 are dominated by pixels with high lightning activity. The OCP values depend on the intensity of convection in each thunderstorm as well as on the phase of the thunderstorm during the TROPOMI overpass (Emersic et al., 2011).

Columns 5 and 6 of Tables 1 and 2 show the median tropospheric VCD of NO$_x$ ($V_{tropNOx}$) and the mean product of the stratospheric VCD of NO$_2$ (~~$V_{tropNOx}$ and~~ $V_{stratNO2}$) times the AMF$_{strat}$ over pixels with deep convection, respectively. Higher values of $V_{stratNO2}$ and the product of $V_{stratNO2}$ times AMF$_{strat}$ for the TROP-DLR research product compared to the TROP-KNMI product can be seen for all cases, except for the case on 30 May. As described in section 2.5, $V_{tropNOx}$ is calculated by using a subtraction between the SCD of NO$_2$ and $V_{stratNO2}$. As $V_{stratNO2}$ is larger for the TROP-DLR research product, we receive lower values of $V_{tropNOx}$ than for the TROP-KNMI research product.

Column 7 shows the mean AMF_{LNOx} over pixels with deep convection for each case. The value of AMF_{LNOx} ranges between 0.34 and 0.80, while the averaged values for the TROP-KNMI and TROP-DLR products are 0.50 and 0.54, respectively. These values are in agreement with typical values reported by Allen et al. (2021a) for thunderstorms observed by TROPOMI over the U.S. (0.41 $\pm$ 0.10) and are similar as the averaged AMF_{LNOx} value in thunderstorms (0.46) reported by Beirle et al. (2009) over the Pacific.

Background-NO$_x$ values as the 30^{th} and the 10^{th} percentile of $V_{tropNOx}$ over non-flashing pixels with deep convection ($V_{tropbck}$) are shown in column 8. As in the case of $V_{tropNOx}$, we receive lower values of $V_{tropbck}$ for TROP-DLR than for the TROP-KNMI research product. Despite similarities in the SCD NO$_2$ from both products, higher $V_{stratNO2}$ values in the TROP-DLR product produce lower values in $V_{tropbck}$ after the subtraction of the stratospheric contribution. There are even some negative values, suggesting that the average stratospheric column exceeding the local vertical column (eq. (3)) or the

tropospheric background exceeding the signal (eq. (2)). $V_{tropbck}$ values show a large variability, although the mean values are of the same order as the background estimated from CARIBIC measurements (0.75 ~~petamolec cm~~$\times 10^{19}$ molec m^{-2}) and from TROPOMI measurements over convective systems with low lightning activity (1.06 ~~petamolec cm~~$\times 10^{19}$ molec m^{-2} for the TROP-KNMI product and 0.37 molec cm^{-2} for the TROP-DLR research product), as detailed in Section 2.6.

The LNO$_x$ PE for each case using ENGLN and EUCLID lightning data are shown in column 9 and 10 of Tables 1 and 2, respectively. We have used the standard deviation over all cases in order to estimate the error of the mean PE. We can see a factor of ∼2 difference between the LNO$_x$ PE using different backgrounds for most of the cases, indicating that the method to estimate the background introduces a significant uncertainty of the results. Using the TROP-KNMI research product, we obtain lower LNO$_x$ PE for ENGLN than for EUCLID (47 ± 33 mol NO$_x$ per flash vs 69 ± 34 mol NO$_x$ per flash). On the contrary, we obtain slightly higher LNO$_x$ PE for ENGLN than for EUCLID when using the TROP-DLR product (58 ± 33 mol NO$_x$ per flash vs 51 ± 25 mol NO$_x$ per flash). The mean LNO$_x$ PE values averaged over ENGLN and EUCLID for the TROP-KNMI and the TROP-DLR products are 58 and 54.5 mol NO$_x$ per flash, respectively. The LNO$_x$ PE value using the TROP-KNMI product is then higher than the value using the TROP-DLR product. We suggest that this slight difference is caused by the higher stratospheric VCD NO$_2$ value in the TROP-DLR product.

The standard deviations of the LNO$_x$ PE derived from the TROP-DLR and the TROP-KNMI products are rather similar, suggesting that the variability in the concentration of NO$_2$ provided by the TROP-DLR NO$_2$ product is similar to the variability provided by the TROP-KNMI product.

The average number of pixels with deep convection and satisfying the quality criterion using the TROP-KNMI product is 370, while it is 758 for the TROP-DLR product. This difference is a consequence of the cut-off employed for both the retrieved cloud fraction and OCP. The cloud fraction over the studied cases is about 30% larger for the TROP-DLR product than for the TROP-KNMI product, while the OCP is about 10% lower for the TROP-DLR product than for the TROP-KNMI product, leading to more pixels with deep convection in the case of TROP-DLR product than in the case of TROP-KNMI product. We have found that using 650 hPa as OCP threshold for the TROP-KNMI product instead of 523 hPa produces a similar total number of pixels with deep convection and satisfying the quality criterium using the TROP-KNMI and the TROP-DLR products. This change in the OCP threshold for the TROP-KNMI product produces a change of only +14% in the LNO$_x$ PE estimates, as more pixels with low convection would be included in the estimation of the background-NO$_x$.

3.2.2 LNO$_x$ PE estimates using fixed background-NO$_x$ values

Let us now estimate the average LNO$_x$ PE over all cases using the *background-NO$_x$ based on days with low lightning activity* as calculated in Section 2.6. Instead of using the $V_{tropbck}$ values of Tables 1 and 2, we use 1.06 ~~petamolec cm~~$\times 10^{19}$ molec m^{-2}, and 0.37 ~~petamolec cm~~$\times 10^{19}$ molec m^{-2} for estimations of the LNO$_x$ PE based on the TROP-KNMI and the TROP-DLR research products, respectively. We obtain 86 ± 63 mol NO$_x$ per flash by using the TROP-KNMI product with ENGLN lightning data, 160 ± 102 mol NO$_x$ per flash by using the TROP-KNMI product with EUCLID lightning data. These values are larger than the mean LNO$_x$ PE using non-flashing pixels (47 ± 33 and 69 ±34 mol NO$_x$ per flash).

By using the background-NO_x based on days with low lightning activity, we calculate 44 $\pm$ 61 mol NO_x per flash by using the TROP-DLR product with ENGLN lightning data and 53 $\pm$ 59 mol NO_x per flash using the TROP-DLR product with EUCLID lightning data. The LNO_x PE estimates based on the TROP-DLR product for the two cases of 7 May and 12 May are negative when using the background-NO_x based on days with low lightning activity, causing lower values of LNO_x PE and larger standard deviations than using the TROP-KNMI product. These values are in agreement with the mean LNO_x PE using non-flashing pixels (58 $\pm$ 33 and 51 $\pm$ 25 mol NO_x per flash).

We calculate the average LNO_x PE over all cases by using the *background-NO_x estimated from CARIBIC measurements* (0.75 ~~petamolec cm~~$\times$ 10^{19} molec m^{-2}), as described in Section 2.6. We obtain 96 $\pm$ 67 mol NO_x per flash using the TROP-KNMI product with ENGLN lightning data, 176 $\pm$ 108 mol NO_x per flash using the TROP-KNMI product with EUCLID lightning data. These values are larger than the mean LNO_x PE using non-flashing pixels (47 $\pm$ 33 and 69 $\pm$34 mol NO_x per flash). Finally, we calculate 17 $\pm$ 48 mol NO_x per flash by using the TROP-DLR product with ENGLN lightning data and 34 $\pm$ 74 mol NO_x per flash using the TROP-DLR product with EUCLID lightning data. Again, the standard deviation of the TROP-DLR LNO_x PE using a fixed value as background-NO_x mixing ratio is lower than in the previous cases, as a consequence of low VCD NO_x of the cases 12 May and 7 May. The LNO_x PE estimates using the TROP-DLR product are negative because the tropospheric VCD of NO_x is lower than the CARIBIC-based estimated background-NO_x (fourth column in Table 2). The obtained TROP-DLR values are lower than the mean LNO_x PE using non-flashing pixels (58 $\pm$ 33 and 51 $\pm$ 25 mol NO_x per flash).

Given that the standard deviation of the received LNO_x PE estimates by using fixed values of the background-NO_x are larger than the means for the TROP-DLR product, we conclude that using fixed values for the background is not adequate in this case-based study. This is a consequence of the observed large variability of the tropospheric VCD of NO_x for each studied thunderstorms. Fixed background values could be useful to estimate the mean LNO_x PE over a number of case studies but less useful to individual case studies.

3.3 Sensitivity analysis and uncertainties

In this section we discuss the most important uncertainties in the estimation of LNO_x PE presented in section 3.2.1. We calculate the uncertainty associated with each parameter by comparing the maximum and the minimum received LNO_x PE values to the mean of the value for the possible choices of that parameter.

Let us begin by discussing the contribution of the employed lightning data to the uncertainty of the LNO_x PE estimates. The mean LNO_x PE of both TROPOMI products (KNMI and DLR) by using ENGLN lightning data is 52.5 mol NO_x per flash, while it is 60 mol NO_x per flash using EUCLID lightning data. Therefore, the *uncertainty introduced by different lightning data sets* is 7%. We have calculated the T-test for the means of the LNO_x PE estimates when using ENGLN and EUCLID lightning data, obtaining a p-value of 0.43. Therefore, we conclude that differences in LNO_x PE using ENTLN and EUCLID are not statistically significant based on the T-test for the means. It is important to mention that the statistical significant is influenced by the population of the sample.

The LNO_x PE estimates by *using different TROPOMI products (KNMI versus DLR)* are not similar, as obtained in section 3.2.1. There is a 23% difference between the LNO_x PE estimates using both TROPOMI products and ENGLN lightning data, and a 35% difference when using EUCLID lightning data. The difference is reduced when using only ENGLN lightning data, whose DE is higher than for EUCLID. The total uncertainty introduced by the choice of the TROPOMI product based on the means LNO_x PE per flash between ENGLN and EUCLID lightning data is only 3%. We obtain a p-value of 0.44 by calculating the T-test for the means of the LNO_x PE estimates when using TROP-KNMI and TROP-DLR, indicating that differences in LNO_x PE using different TROPOMI products are not statistically significant.

As shown in Tables 1 and 2, the estimation of the ~~*background-NO_x*~~ background-NO_x as the 30^{th} or as the 10^{th} percentile of $V_{tropNOx}$ over non-flashing pixels with deep convection can significantly influence the LNO_x PE estimates. The average LNO_x PE between both TROPOMI products using the 30^{th} percentile of $V_{tropNOx}$ is 42 mol NO_x per flash, while it is 70 mol NO_x per flash using the 10^{th} percentile of $V_{tropNOx}$. Therefore, the choice of the background-NO_x method contributes to the uncertainty of 29%. The p-value obtained by calculating the T-test for the means of the LNO_x PE estimates by using the 30^{th} or the 10^{th} percentile of $V_{tropNOx}$ over non-flashing pixels with deep convection as background-NO_x is lower than 0.05, which indicates that differences in LNO_x PE using different methods to estimate the background-NO_x products are statistically significant.

The *DE of the used LLS* can also contribute to the uncertainty of the LNO_x PE estimates. As explained in section 2.2, we obtain a DE for ENGLN over the Pyrenees of 0.676 ± 0.12 (ranging between 0.556 and 0.769). The obtained mean LNO_x PE using both TROPOMI products and a DE of 0.769 is 59 mol NO_x per flash, while it is 43 mol NO_x per flash when using a DE of 0.556. Therefore, the uncertainty of the DE of ENGLN contributes to a LNO_x PE uncertainty of 17%. For EUCLID, we obtain a DE of 0.27 ± 0.12. The obtained mean LNO_x PE using EUCLID data corrected by a DE of 0.40 is 86 mol NO_x per flash, while it is 33 mol NO_x per flash when using a DE of 0.15. Therefore, the uncertainty of the DE of EUCLID contributes to a LNO_x PE uncertainty of 62%. The contribution of the DE of EUCLID to the uncertainty is higher than the contribution of the DE of ENGLN because the DE of EUCLID is significantly lower than the DE of ENGLN.

The *lifetime of NO_x* in the near field of convection (τ) is another parameter that can introduce uncertainty to the LNO_x PE estimates. We have used 3 h, but it can vary between 2 and 12 h (Nault et al., 2017; Allen et al., 2021a). We have performed the LNO_x PE calculations using the TROPOMI products and ENGLN lightning data and setting τ = 12 h as an upper limit keeping the time windows used at 5 h, obtaining a mean LNO_x PE of 38 mol NO_x per flash. Given that the LNO_x PE with τ = 3 h is 52.5 mol NO_x per flash, we estimate that τ contributes to the uncertainty of the LNO_x PE by about 18%.

The *time window before the TROPOMI overpass*, that is used to count the total number of lightning flashes contributing to fresh-produced LNO_x, can also be a source of uncertainty. We have calculated the LNO_x PE estimates using a time window of 1 h instead of 5 h in order to get an estimation of the uncertainty introduced by the time window. We receive 88 mol NO_x per flash as the mean value by using the TROP-KNMI and the TROP-DLR products and ENGLN lightning data. The LNO_x PE estimations using the same TROPOMI products and lightning data with a time window of 5 h was 52.5 mol NO_x per flash. According to our estimations, the time window contribution to the uncertainty of the LNO_x PE is about 29%. We do not

Table 3. Sources of differences in the mean LNO_x PE estimates.

Source of difference	Influence on the LNO_x PE estimate
Lightning data set (ENGLN or EUCLID)	7%
TROPOMI product (DLR or KNMI v2.1)	3%
Background-NO_x estimation (10% or 30% of non-flashing pixels)	29%
Lightning detection system DE using ENGLN	17%
Lightning detection system DE using EUCLID	62%
Lifetime of NO_x in the near field of convection (τ)	18%
Time window before the TROPOMI overpass	29%
Other (lightning parameterization, scattering weights, deep convection definition)	30%
Overall uncertainty using ENGLN	57%
Overall uncertainty using EUCLID	83%

perform calculations using a larger time window, because studying the transport of LNO_x at longer time scales is out of the scope of this work.

The sources of differences in the LNO_x PE estimation evaluated in this study are summarized in Table 3. As discussed in previous studies (e.g., Pickering et al., 2016; Allen et al., 2019; Lapierre et al., 2020; Zhang et al., 2020; Allen et al., 2021a), there are other possible sources of uncertainty, such as the calculation of the AMF (LNO_x profile type and lightning parameterization and NO_x/NO_2 ratios in the simulations, scattering weights calculations) contributing to the uncertainty of about 30% or the method to select the OCP to be used for the definition of deep convection, contributing to the uncertainty of about 10%, or other systematic errors in the retrieval algorithms of TROPOMI. However, estimates of the influence of these parameters for the uncertainty of LNO_x PE on the particular area of the Pyrenees is out of the scope of this paper, as we do not expect them to be dependent on the studied area.

We can estimate the overall LNO_x PE uncertainty by summing the uncertainties in PE collected in Table 3. We obtain an overall LNO_x PE uncertainty of 57% using ENGLN lightning data and 83% using EUCLID lightning data.

4 Discussion

Previous studies have used OMI NO_2 measurements to estimate the LNO_x PE over different regions, as shown in Table 4. Pickering et al. (2016) reported a LNO_x PE of 80 $\pm$ 45 mol per flash over the Gulf of Mexico. Bucsela et al. (2019) systematically estimated the LNO_x PE over mid-latitudes, obtaining an average LNO_x PE of 180 $\pm$ 100 mol per flash. Interestingly, Bucsela et al. (2019) (see Table 1) found a lower LNO_x PE in Europe (150 $\pm$ 90 mol per flash). Allen et al. (2019) reported a mean LNO_x PE over the tropics of 170 $\pm$ 100 mol per flash. Lapierre et al. (2020) reported a LNO_x PE over the USA of $\sim$24 mol per flash (estimated from mol per stroke calculations), while Zhang et al. (2020) reported 90 $\pm$ 50 mol per flash over the USA. Recently, Allen et al. (2021a) have estimated the LNO_x PE in 29 thunderstorms over the USA by using new TROPOMI NO_2 data, finding a LNO_x PE of 120 $\pm$ 50 mol per flash based on the use of ENGLN lightning data. We have calculated the T-test for the means of the LNO_x PE estimates when using ENGLN lightning data together with the TROP-KNMI product and

Table 4. Some recent LNO_x PE estimates.

Area	Instrument	LNO_x PE estimate (mol per flash)	Reference
Gulf of Mexico	OMI	80 ± 45	Pickering et al. (2016)
Mid-latitudes	OMI	180 ± 100 mol	Bucsela et al. (2019)
Tropics	OMI	170 ± 100	Allen et al. (2019)
USA	OMI	$\sim$24 mol	Lapierre et al. (2020)
USA	OMI	90 ± 50	Zhang et al. (2020)
USA	TROPOMI	120 ± 50	Allen et al. (2021a)
Pyrenees and Ebro Valley	TROPOMI	58 ± 44	This work

the LNO_x PE estimates provided by Allen et al. (2021a) when using ENGLN lightning data, obtaining a p-value lower than 0.05. Therefore, we conclude that differences in LNO_x PE between the Pyrenees and the U.S. are statistically significant.

We have used the LNO_x PE algorithm employed by Pickering et al. (2016); Bucsela et al. (2019); Allen et al. (2019) and Allen et al. (2021a) to provide new LNO_x PE estimate based on TROPOMI NO_2 measurements over the Pyrenees. We obtain 47 ± 33 (69 ± 34) mol NO_x per flash using the TROP-KNMI research product and ENGLN (EUCLID) lightning data and 58 ± 33 (51 ± 25 mol NO_x) mol NO_x per flash using TROP-DLR product and ENGLN (EUCLID) lightning data. Our mean LNO_x PE estimates are slightly lower than the LNO_x PE reported by Pickering et al. (e.g., 2016); Allen et al. (e.g., 2019); Zhang et al. (e.g., 2020); Allen et al. (e.g., 2021a) and a factor of $\sim$2 higher as determined by Lapierre et al. (2020). The employed method uses only TROPOMI measurements over cloudy pixels to estimate fresh-produced LNO_x. As a consequence, part of the LNO_x produced before the TROPOMI overpass can be overlooked. Consequently, the obtained LNO_x PE can be biased low.

Let us now compare our results with TROPOMI-based estimates by Allen et al. (2021a) over the USA using ENGLN lightning data (120 ± 50 mol). We obtain lower LNO_x PE estimates, which is in agreement with Bucsela et al. (2019), who reported a lower LNO_x PE over Europe than over the USA. We estimate a mean tropospheric VCD of NO_x of 3.5 ~~petamolec cm~~$\times 10^{19}$ molec m^{-2} from the TROP-KNMI product. Allen et al. (2021a) reported a slightly higher mean VCD of NO_x of 4.4 ~~petamolec cm~~$\times 10^{19}$ molec m^{-2} from the TROP-KNMI product. The Pyrenees are a low contaminated area, which explains that the tropospheric VCD of NO_x is lower than for the 29 cases studied by Allen et al. (2021a) over the USA. We have also found comparable influence of the background-NO_x on the uncertainty of our results than Allen et al. (2021a), (29% vs 22.5%). The explanation of this difference can be that Allen et al. (2021a) analyzed 29 cases, while in this study we have analyzed only 8 cases.

The obtained LNO_x PE are significantly influenced by the TROPOMI (KNMI and DLR) and the lightning (ENGLN and EUCLID) data sets. The difference between the LNO_x PE calculated by using the TROP-KNMI and the TROP-DLR products together with the ENGLN lightning data is 3%. There is a factor of 3.5 difference in the estimated median tropospheric VCD of NO_x using the TROP-KNMI product (3.5 ~~petamolec cm~~$\times 10^{19}$ molec m^{-2}) and the TROP-DLR product (0.96 ~~petamolec cm~~$\times 10^{19}$ molec m^{-2}), while the differences in the provided mean stratospheric VCD of NO_2 over pixels with deep convection is 14% (7.3 and 8.3 ~~petamolec cm~~$\times 10^{19}$ molec m^{-2} for the TROP-KNMI and the TROP-DLR products, respectively). The background-NO_x is estimated from non-flashing pixels, leading to a similar $V_{tropLNOx}$ and LNO_x PE values. However, using

a fixed value for the background-NO_x produces significantly lower LNO_x PE for the TROP-DLR product than for the TROP-KNMI product, as a consequence of the lower tropospheric VCD of NO_x obtained from the TROP-DLR product.

Despite significant differences in the DE of ENGLN and EUCLID in the studied area, we have not found significant differences in the mean estimation of the LNO_x PE using lightning data from both networks after correction with the DE. The LNO_x PE estimates using the TROP-DLR product together with ENGLN and EUCLID lightning data are nearly similar (58 $\pm$ 33 mol NO_x per flash and 51 $\pm$ 25 mol NO_x, respectively). However, we have found that the LNO_x PE obtained using the TROP-KNMI product are different for ENGLN (47 $\pm$ 33 mol per flash) and EUCLID data (69 $\pm$ 34 mol per flash). We have found that the received LNO_x PE using ENGLN ranges between 39 and 59 mol NO_x per flash after correction by the DE 0.676 $\pm$ 0.12, while the calculated LNO_x PE using EUCLID ranges between 33 and 86 mol NO_x per flash after correction by the DE 0.27 $\pm$ 0.12. Therefore, we conclude that the higher DE of ENGLN provides more precise LNO_x PE than EUCLID in the studied area.

5 Conclusions

We have estimated the LNO_x PE over the Pyrenees, a European region with high lightning activity and relatively low concentration of background-NO_x. We have used two lightning data sets (ENGLN and EUCLID) and two TROPOMI NO_2 and cloud products (DLR and KNMI v2.1) in this study. The main conclusions of this work are as follows:

1. We obtain 47 $\pm$ 33 mol NO_x per flash using the TROP-KNMI research product and ENGLN lightning data, 69 $\pm$ 34 mol NO_x per flash using TROP-KNMI research product and EUCLID lightning data, 58 $\pm$ 33 mol NO_x per flash using the TROP-DLR product and ENGLN lightning data and 51 $\pm$ 25 mol NO_x per flash by using TROP-DLR product and EUCLID lightning data. Overall, the obtained LNO_x PE ranges between 14 and 103 mol NO_x per flash. These estimates are lower than the globally averaged LNO_x PE (250 $\pm$ 150 mol per flash) estimated by Schumann and Huntrieser (2007) and the LNO_x PE estimates from the TROPOMI measurements and ENGLN lightning data in the USA by Allen et al. (2021a) (120 $\pm$ 50 mol per flash).

2. We have used different methods to estimate the background-NO_x, i.e., the background-NO_x from non-flashing pixels and from measurements over days with low lightning activity. When using ENGLN lightning data, we have found that the most important source of uncertainty for LNO_x PE is the estimation of the background-NO_x (about 29%), similar as by the time window prior to the TROPOMI overpass time used to collect the lightning data (about 29%). The overall uncertainty when using ENGLN lightning data is 57%. When using EUCLID lightning data, the most important source of uncertainty is the DE of EUCLID (about 62%), while the overall uncertainty when using EUCLID lightning data is 83%.

3. The estimated median tropospheric VCD of NO_x in convective systems after subtraction of the stratospheric NO_2contribution is a factor of 3.5 lower for the TROP-DLR product than for the TROP-KNMI product as a consequence of larger stratospheric VCD of NO_2 in the TROP-DLR product over pixels with deep convection.

4. The ~~mean LNO_x PE obtained from ENGLN and EUCLID lightning data are not considerably different in comparison to differences obtained by using different methods to estimate~~ uncertainty introduced by the estimate of the background-NO_x is considerably larger than the uncertainty introduced by the choice of the lightning data set (ENGLN or EUCLID).

This paper reports on partly new and partly established methods to estimate LNO_x PE. It confirms that the uncertainty in the calculation of LNO_x PE is still high, even when using high resolution measurements from TROPOMI. It also suggests that the LNO_x PE vary substantially between different regions, as suggested by a comparison between our results and recent OMI- and TROPOMI-based LNO_x PE over the USA (Lapierre et al., 2020; Allen et al., 2021a). This study also shows that differences in LNO_x PE estimates can be caused by the different lightning systems.

The launch of the Meteosat Third Generation (MTG) geostationary satellites of the EUropean organization for the exploitation of METeorological SATellites (EUMETSAT) in 2022 will for the first time provide a continuous monitoring of the occurrence of lightning flashes from space in Europe and Africa through the instrument Lightning Imager (LI) from 2023 onwards (Stuhlmann et al., 2005). Lightning data from the MTG-LI can contribute to improve LNO_x estimates over the studied region, Europe and Africa. In fact, lightning data from the geostationary GLM has already contributed to new LNO_x PE estimations over America (Allen et al., 2021b, a). High temporal and spatial resolution observations from the Geostationary Environment Monitoring Spectrometer (GEMS) and the future NO_2 retrieving instruments on-board geostationary satellites, such as the SENTINEL-4 GEO in 2023 (Courrèges-Lacoste et al., 2017), the Tropospheric Emissions: Monitoring of Pollution (TEMPO) (Zoogman et al., 2017) in 2022 will also contribute to provide more data to estimate the LNO_x PE over Asia, North America, Europe and Africa.

Data availability. All data used in this paper are directly available after a request is made to authors F. J. P. I (FranciscoJavier.Perez-Invernon@dlr.de) or H. H. (Heidi.Huntrieser@dlr.de). The official TROPOMI data are available via ESA's public data hub (https://s5phub.copernicus.eu/). The ERA5 meteorological data are freely accessible through Copernicus Climate Change Service (C3S) (2017): ERA5: Fifth generation of ECMWF atmospheric reanalyses of the global climate Copernicus Climate Change Service Climate Data Store (CDS) (https://cds.climate.copernicus.eu/cdsapp). ENGLN and EUCLID data were obtained freely by request from Earth Networks (https://www.earthnetworks.com) and AEMET (http://www.aemet.es/es/datos_abiertos), respectively. ISS-LIS data can be freely downloaded from https://ghrc.nsstc.nasa.gov/lightning/data/data_lis_iss.html. IAGOS-CARIBIC data can be freely downloaded from https://www.iagos.org/iagos-data/.

A Appendix A: Acronym list of physical quantities

A: Area of deep convection

AMF: Ais mass factor

AMF_{LNOx}: Ais mass factor used to convert tropospheric slant columnsdensity of NO_2 to vertical column density of LNO_x

AMF_{strat}: Stratosferic air mass factor from TROPOMI product

DE: Detection efficiency

F: Flashes contributing to LNO_x column

N_A: Avogadro's number

OCP: Optical centroid pressure

PE: Production efficiency

SCD: Slant column density

S_{NO2}: Slant column density of NO_2

t_i: Time of individual flash

τ: Chemical lifetime of LNO_x

VCD: Vertical column density

$V_{tropbkgn}$: Vertical column of tropospheric NO_x due to non-recent lightning

$V_{tropLNOx}$: Vertical column of tropospheric NO_x due to recent lightning

$V_{tropNOx}$: Vertical column of tropospheric NO_x

Author contributions. F.J.P.I.: Conceptualization, methodology, validation, formal analysis, investigation, data curation, writing—original draft. H.H.: Conceptualization, methodology, validation, formal analysis, supervision, investigation, writing—review and editing. T. E.: Validation, data curation. D. L., P. V. and S.L: Validation, data curation, preparation of the TROP-DLR product. D. A., K. P. and E. B: Methodology, validation, formal analysis. P. J.: Validation, supervision of EMAC simulations. J. v. G and H. E: Validation, data curation, preparation of the TROP-KNMI product. F.J.G.V., S. S. and J. L.: Data curation, validation, preparation of the ENGLN lightning data.

Competing interests. Authors declare no competing interests.

Acknowledgements. The authors would like to thank DLR and KNMI for providing TROPOMI research NO_2 and cloud data, Earth Networks for providing ENTGN lightning data, Spanish State Meteorological Agency (AEMET) for providing EUCLID lightning data, NASA for providing ISS-LIS lightning data, ECMWF for providing the data of ERA5 forecasting models and IAGOS Research Infrastructure for providing NO data. The EMAC simulations have been performed at the German Climate Computing Centre (DKRZ) through support from the Bundesministerium für Bildung und Forschung (BMBF). DKRZ and its scientific steering committee are gratefully acknowledged for providing the HPC and data archiving resources.Authors would also like to thank Volker Grewe (Deutsches Zentrum für Luft-und Raumfahrt, DLR) for providing valuable comments on this manuscript.

FJPI acknowledges the sponsorship provided by the Federal Ministry for Education and Research of Germany through the Alexander von Humboldt Foundation. Additionally, this work was supported by the Spanish Ministry of Science and Innovation, under projects PID2019-109269RB-C43 and FEDER program. SS acknowledges a PhD research contract through the project PID2019-109269RB-C43. FJGV and SS acknowledge financial support from the State Agency for Research of the Spanish MCIU through the 'Center of Excellence Severo Ochoa' award for the Instituto de Astrofísica de Andaluca (SEV-2017-0709).

References

Allen, D., Pickering, K. E., Bucsela, E., Van Geffen, J., Lapierre, J., Koshak, W., and Eskes, H.: Observations of Lightning NO_x Production From Tropospheric Monitoring Instrument Case Studies Over the United States, J. Geophys. Res. Atmos., 126, e2020JD034 174, https://doi.org/10.1029/2020JD034174, 2021a.

Allen, D. J., Pickering, K. E., Bucsela, E., Krotkov, N., and Holzworth, R.: Lightning NO_x production in the tropics as determined using OMI NO_2 retrievals and WWLLN stroke data, J. Geophys. Res. Atmos., 124, 13 498–13 518, https://doi.org/10.1029/2019JD030561., 2019.

Allen, D. J., Pickering, K. E., Lamsal, L., Mach, D. M., Quick, M. G., Lapierre, J., Janz, S., Koshak, W., Kowalewski, M., and Blakeslee, R.: Observations of Lightning NO_x Production From GOES R Post Launch Test Field Campaign Flights, J. Geophys. Res. Atmos., 126, e33 769, https://doi.org/10.1029/2020JD033769, 2021b.

Anderson, G. and Klugmann, D.: A European lightning density analysis using 5 years of ATDnet data, Nat. Hazards Earth Syst. Sci., 14, 815–829, https://doi.org/10.5194/nhess-14-815-2014, 2014.

Beirle, S., Salzmann, M., Lawrence, M., and Wagner, T.: Sensitivity of satellite observations for freshly produced lightning NO_x, Atmos. Chem. Phys., 9, 1077–1094, https://doi.org/10.5194/acp-9-1077-2009, 2009.

Beirle, S., Huntrieser, H., and Wagner, T.: Direct satellite observation of lightning-produced NO_x, Atmos. Chem. and Phys., 10, 10 965–10 986, https://doi.org/10.5194/acp-10-10965-2010, 2010.

Bitzer, P. M. and Christian, H. J.: Timing uncertainty of the lightning imaging sensor, J. Atmos. Ocean. Technol., 32, 453–460, https://doi.org/10.1175/JTECH-D-13-00177.1, 2015.

Bitzer, P. M., Burchfield, J. C., and Christian, H. J.: A Bayesian approach to assess the performance of lightning detection systems, J. Atmos. Ocean. Technol., 33, 563–578, https://doi.org/10.1175/JTECH-D-15-0032.1, 2016.

Blakeslee, R., Lang, T., Koshak, W., Buechler, D., Gatlin, P., Mach, D., Stano, G., Virts, K., Walker, T., Cecil, D., et al.: Three years of the Lightning Imaging Sensor onboard the International Space Station: Expanded Global Coverage and Enhanced Applications, Earth Space Sci. Open Archive, 35812, 83, https://doi.org/10.1029/2020JD032918, 2020.

Boersma, K. F., Eskes, H. J., Richter, A., Smedt, I. D., Lorente, A., Beirle, S., Van Geffen, J. H., Zara, M., Peters, E., Roozendael, M. V., et al.: Improving algorithms and uncertainty estimates for satellite NO 2 retrievals: results from the quality assurance for the essential climate variables (QA4ECV) project, Atmos. Meas. Tech., 11, 6651–6678, https://doi.org/10.5194/amt-11-6651-2018, 2018.

Brenninkmeijer, C. A. M., Crutzen, P., Boumard, F., Dauer, T., Dix, B., Ebinghaus, R., Filippi, D., Fischer, H., Franke, H., Frieβ, U., Heintzenberg, J., Helleis, F., Hermann, M., Kock, H. H., Koeppel, C., Lelieveld, J., Leuenberger, M., Martinsson, B. G., Miemczyk, S., Moret, H. P., Nguyen, H. N., Nyfeler, P., Oram, D., O'Sullivan, D., Penkett, S., Platt, U., Pupek, M., Ramonet, M., Randa, B., Reichelt, M., Rhee, T. S., Rohwer, J., Rosenfeld, K., Scharffe, D., Schlager, H., Schumann, U., Slemr, F., Sprung, D., Stock, P., Thaler, R., Valentino, F., van Velthoven, P., Waibel, A., Wandel, A., Waschitschek, K., Wiedensohler, A., Xueref-Remy, I., Zahn, A., Zech, U., and Ziereis, H.: Civil Aircraft for the regular investigation of the atmosphere based on an instrumented container: The new CARIBIC system, Atmos. Chem. Phys., 7, 4953–4976, https://doi.org/10.5194/acp-7-4953-2007, 2007.

Bucsela, E., Krotkov, N., Celarier, E., Lamsal, L., Swartz, W., Bhartia, P., Boersma, K., Veefkind, J., Gleason, J., and Pickering, K.: A new stratospheric and tropospheric NO_2 retrieval algorithm for nadir-viewing satellite instruments: applications to OMI, Atmos. Meas. Tech., 6, 2607–2626, https://doi.org/10.5194/amt-6-2607-2013, 2013.

Bucsela, E. J., Pickering, K. E., Allen, D. J., Holzworth, R. H., and Krotkov, N. A.: Midlatitude lightning NO_x production efficiency inferred from OMI and WWLLN data, J. Geophys. Res. Atmos., 124, 13 475–13 497, https://doi.org/10.1029/2018JD029824, 2019.

Cecil, D. J., Buechler, D. E., and Blakeslee, R. J.: Gridded lightning climatology from TRMM-LIS and OTD: Dataset description, Atmos. Res., 135, 404–414, https://doi.org/10.1016/j.atmosres.2012.06.028, 2014.

Christian, H. J., Blakeslee, R. J., Boccippio, D. J., Boeck, W. L., Buechler, D. E., Driscoll, K. T., Goodman, S. J., Hall, J. M., Koshak, J. M., Mach, D. M., and Stewart, M. F.: Global frequency and distribution of lightning as observed from space by the Optical Transient Detector, J. Geophys. Res., 108, ACL 4–1, https://doi.org/10.1029/2002JD002347, 2003.

Courrèges-Lacoste, G. B., Sallusti, M., Bulsa, G., Bagnasco, G., Veihelmann, B., Riedl, S., Smith, D., and Maurer, R.: The Copernicus Sentinel 4 mission: a geostationary imaging UVN spectrometer for air quality monitoring, in: Sensors, Systems, and Next-Generation Satellites XXI, vol. 10423, p. 1042307, International Society for Optics and Photonics, 2017.

Dave, J. V.: Multiple Scattering in a Non-Homogeneous, Rayleigh Atmosphere, J. Atmos. Sci., 22, 273–279, https://doi.org/10.1175/1520-0469, 1965.

Deckert, R., Jöckel, P., Grewe, V., Gottschaldt, K.-D., and Hoor, P.: A quasi chemistry-transport model mode for EMAC, Geosci. Model. Dev., 4, 195–206, https://doi.org/10.5194/gmd-4-195-2011, 2011.

Emersic, C., Heinselman, P. L., MacGorman, D. R., and Bruning, E. C.: Lightning Activity in a Hail-Producing Storm Observed with Phased-Array Radar, Mon. Weather Rev., 139, 1809 – 1825, https://doi.org/10.1175/2010MWR3574.1, 2011.

Esteban, P., Martin-Vide, J., and Mases, M.: Daily atmospheric circulation catalogue for western Europe using multivariate techniques, Int. J. Climatol., 26, 1501–1515, https://doi.org/10.1002/joc.1391, 2006.

Gordillo-Vázquez, F. J., Pérez-Invernón, F. J., Huntrieser, H., and Smith, A. K.: Comparison of Six Lightning Parameterizations in CAM5 and the Impact on Global Atmospheric Chemistry, Earth Space Sci., 6, 2317–2346, https://doi.org/10.1029/2019EA000873, 2019.

Grewe, V., Brunner, D., Dameris, M., Grenfell, J., Hein, R., Shindell, D., and Staehelin, J.: Origin and variability of upper tropospheric nitrogen oxides and ozone at northern mid-latitudes, Atmos. Environ., 35, 3421–3433, https://doi.org/10.1016/S1352-2310(01)00134-0, 2001.

Huntrieser, H., Feigl, C., Schlager, H., Schröder, F., Gerbig, C., Van Velthoven, P., Flatøy, F., Théry, C., Petzold, A., Höller, H., et al.: Airborne measurements of NO_x, tracer species, and small particles during the European Lightning Nitrogen Oxides Experiment, J. Geophys. Res. Atmos., 107, ACH–5, https://doi.org/10.1029/2000JD000209, 2002.

Huntrieser, H., Lichtenstern, M., Scheibe, M., Aufmhoff, H., Schlager, H., Pucik, T., Minikin, A., Weinzierl, B., Heimerl, K., Pollack, I., et al.: Injection of lightning-produced NO_x, water vapor, wildfire emissions, and stratospheric air to the UT/LS as observed from DC3 measurements, J. Geophys. Res. Atmos., 121, 6638–6668, https://doi.org/10.1002/2015JD024273, 2016.

Hutchins, M. L., Holzworth, R. H., Rodger, C., Heckman, S., and Brundell, J. B.: WWLLN absolute detection efficiencies and the global lightning source function, in: EGU General Assembly Conference Abstracts, p. 12917, 2012.

Jöckel, P., Tost, H., Pozzer, A., Kunze, M., Kirner, O., Brenninkmeijer, C. A., Brinkop, S., Cai, D. S., Dyroff, C., Eckstein, J., et al.: Earth system chemistry integrated modelling (ESCiMo) with the modular earth submodel system (MESSy) version 2.51, Geosci. Model. Dev., 9, 1153–1200, https://doi.org/10.5194/gmd-9-1153-2016, 2016.

Kieu, N., Gordillo-Vázquez, F. J., Passas, M., Sánchez, J., and Pérez-Invernón, F. J.: High-speed spectroscopy of lightning-like discharges: evidence of molecular optical emissions, J. Geophys. Res. Atmos., p. e2021JD035016, https://doi.org/10.1029/2021JD035016, 2021.

Koelemeijer, R., Stammes, P., Hovenier, J., and De Haan, J.: A fast method for retrieval of cloud parameters using oxygen A band measurements from the Global Ozone Monitoring Experiment, J. Geophys. Res. Atmos., 106, 3475–3490, https://doi.org/10.1029/2000JD900657, 2001.

Labrador, L., Kuhlmann, R. v., and Lawrence, M.: The effects of lightning-produced NO_x and its vertical distribution on atmospheric chemistry: Sensitivity simulations with MATCH-MPIC, Atmos. Chem. Phys., 5, 1815–1834, https://doi.org/10.5194/acp-5-1815-2005, 2005.

Lapierre, J. L., Laughner, J. L., Geddes, J. A., Koshak, W. J., Cohen, R. C., and Pusede, S. E.: Observing US regional variability in lightning NO_2 production rates, J. Geophys. Res. Atmos., 125, e2019JD031 362, https://doi.org/10.1029/2019JD031362, 2020.

Lindfors, A. V., Kujanpää, J., Kalakoski, N., Heikkilä, A., Lakkala, K., Mielonen, T., Sneep, M., Krotkov, N. A., Arola, A., and Tamminen, J.: The TROPOMI surface UV algorithm, Atmos. Meas. Tech., 11, 997–1008, https://doi.org/10.5194/amt-11-997-2018, 2018.

Liu, C. and Heckman, S.: The application of total lightning detection and cell tracking for severe weather prediction, in: 91st Bull. Am. Meteorol. Soc. Annual Meeting, pp. 1–10, 2011.

Liu, C., Sloop, C., and Heckman, S.: Application of lightning in predicting high impact weather, in: Preprints, WMO Technical conference on meteorological and environmental instruments and methods of observation, July 7, vol. 9, 2014.

Liu, S., Valks, P., Pinardi, G., Xu, J., Chan, K. L., Argyrouli, A., Lutz, R., Beirle, S., Khorsandi, E., Baier, F., et al.: An improved tropospheric NO_2 column retrieval algorithm for TROPOMI over Europe, Atmos. Meas. Tech., pp. 1–43, https://doi.org/10.5194/amt-2021-39, 2021.

Loyola, D. G., Gimeno García, S., Lutz, R., Argyrouli, A., Romahn, F., Spurr, R. J., Pedergnana, M., Doicu, A., Molina García, V., and Schüssler, O.: The operational cloud retrieval algorithms from TROPOMI on board Sentinel-5 Precursor, Atmos. Meas. Tech., 11, 409–427, https://doi.org/10.5194/amt-11-409-2018, 2018.

Ludewig, A., Kleipool, Q., Bartstra, R., Landzaat, R., Leloux, J., Loots, E., Meijering, P., van der Plas, E., Rozemeijer, N., Vonk, F., and Veefkind, P.: In-flight calibration results of the TROPOMI payload on board the Sentinel-5 Precursor satellite, Atmos. Meas. Tech., 13, 3561–3580, https://doi.org/10.5194/amt-13-3561-2020, 2020.

Mach, D. M., Christian, H. J., Blakeslee, R. J., Boccippio, D. J., Goodman, S. J., and Boeck, W. L.: Performance assessment of the optical transient detector and lightning imaging sensor, J. Geophys. Res. Atmos., 112, https://doi.org/10.1029/2006JD007787, 2007.

Marais, E. A., Jacob, D. J., Choi, S., Joiner, J., Belmonte-Rivas, M., Cohen, R. C., Beirle, S., Murray, L. T., Schiferl, L. D., Shah, V., and Jaeglé, L.: Nitrogen oxides in the global upper troposphere: interpreting cloud-sliced NO_2 observations from the OMI satellite instrument, Atmos. Chem. Phys., 18, 17 017–17 027, https://doi.org/10.5194/acp-18-17017-2018, 2018.

Marais, E. A., Roberts, J. F., Ryan, R. G., Eskes, H., Boersma, K. F., Choi, S., Joiner, J., Abuhassan, N., Redondas, A., Grutter, M., et al.: New observations of NO_2 in the upper troposphere from TROPOMI, Atmos. Meas. Tech., 14, 2389–2408, https://doi.org/10.5194/amt-14-2389-2021, 2021.

Marchand, M., Hilburn, K., and Miller, S. D.: Geostationary Lightning Mapper and Earth Networks lightning detection over the contiguous United States and dependence on flash characteristics, J. Geophys. Res. Atmos., 124, 11 552–11 567, https://doi.org/10.1029/2019JD031039, 2019.

Molinie, G., Soula, S., and Chauzy, S.: Cloud-to-ground lightning activity and radar observations of storms in the Pyrénées range area, Q. J. R. Meteorol. Soc., 125, 3103–3122, https://doi.org/10.1002/qj.49712556015, 1999.

Murray, L. T., Jacob, D. J., Logan, J. A., Hudman, R. C., and Koshak, W. J.: Optimized regional and interannual variability of lightning in a global chemical transport model constrained by LIS/OTD satellite data, J. Geophys. Res. Atmos., 117, https://doi.org/10.1029/2012JD017934, 2012.

Myriokefalitakis, S., Daskalakis, N., Gkouvousis, A., Hilboll, A., van Noije, T., Williams, J. E., Le Sager, P., Huijnen, V., Houweling, S., Bergman, T., Nüß, J. R., Vrekoussis, M., Kanakidou, M., and Krol, M. C.: Description and evaluation of a detailed gas-phase chemistry

scheme in the TM5-MP global chemistry transport model (r112), Geosci. Model. Dev., 13, 5507–5548, https://doi.org/10.5194/gmd-13-5507-2020, 2020.

National Aeronautics and Space Administration: Collection: Blue Marble - NASA Visible Earth, https://visibleearth.nasa.gov/collection/1484/blue-marble, 2021.

Nault, B. A., Laughner, J. L., Wooldridge, P. J., Crounse, J. D., Dibb, J., Diskin, G., Peischl, J., Podolske, J. R., Pollack, I. B., Ryerson, T. B., Scheuer, E., Wennberg, P. O., and Cohen, R. C.: Lightning NO_x Emissions: Reconciling Measured and Modeled Estimates With Updated NO_x Chemistry, Geophys. Res. Lett., 44, 9479–9488, https://doi.org/10.1002/2017GL074436, 10.1002/2017GL074436, 2017GL074436, 2017.

Pan, L. L., Homeyer, C. R., Honomichl, S., Ridley, B. A., Weisman, M., Barth, M. C., Hair, J. W., Fenn, M. A., Butler, C., Diskin, G. S., et al.: Thunderstorms enhance tropospheric ozone by wrapping and shedding stratospheric air, Geophys. Res. Lett., 41, 7785–7790, https://doi.org/10.1002/2014GL061921, 2014.

Pickering, K. E., Wang, Y., Tao, W.-K., Price, C., and Müller, J.-F.: Vertical distributions of lightning NO_x for use in regional and global chemical transport models, J. Geophys. Res. Atmos., 103, 31 203–31 216, https://doi.org/10.1029/98JD02651, 1998.

Pickering, K. E., Bucsela, E., Allen, D., Ring, A., Holzworth, R., and Krotkov, N.: Estimates of lightning NO_x production based on OMI NO_2 observations over the Gulf of Mexico, J. Geophys. Res. Atmos., 121, 8668–8691, https://doi.org/10.1002/2015JD024179, 2016.

Pineda, N., Esteban, P., Trapero, L., Soler, X., and Beck, C.: Circulation types related to lightning activity over Catalonia and the Principality of Andorra, Phys. Chem. Earth, Parts A/B/C, 35, 469–476, https://doi.org/10.1016/j.pce.2009.12.009, 2010.

Poelman, D. R. and Schulz, W.: Comparing lightning observations of the ground-based European lightning location system EUCLID and the space-based Lightning Imaging Sensor (LIS) on the International Space Station (ISS), Atmos. Meas. Tech., VOLUME = 13, YEAR = 2020, NUMBER = 6, PAGES = 2965–2977, URL = https://amt.copernicus.org/articles/13/2965/2020/, DOI = 10.5194/amt-13-2965-2020.

Price, C., Penner, J., and Prather, M.: NO_x from lightning: 1. Global distribution based on lightning physics, J. Geophys. Res., 102, 5929, https://doi.org/10.1029/96JD03504, 1997.

Ripoll, J.-F., Zinn, J., Colestock, P. L., and Jeffery, C. A.: On the dynamics of hot air plasmas related to lightning discharges: 2. Electrodynamics, J. Geophys. Res. Atmos., 119, 9218–9235, https://doi.org/10.1002/2013JD020067, 2014a.

Ripoll, J.-F., Zinn, J., Jeffery, C. A., and Colestock, P. L.: On the dynamics of hot air plasmas related to lightning discharges: 1. Gas dynamics, J. Geophys. Res. Atmos., 119, 9196–9217, https://doi.org/10.1002/2013JD020068, 2014b.

Schulz, W., Diendorfer, G., Pedeboy, S., and Poelman, D. R.: The European lightning location system EUCLID–Part 1: Performance analysis and validation, Nat. Hazards Earth Syst. Sci., 16, 595–605, https://doi.org/10.5194/nhess-16-595-2016, 2016.

Schumann, U. and Huntrieser, H.: The global lightning-induced nitrogen oxides source, Atmos. Chem. Phys., 7, 3823, https://doi.org/10.5194/acp-7-3823-2007, 2007.

Silvern, R., Jacob, D., Travis, K., Sherwen, T., Evans, M., Cohen, R., Laughner, J., Hall, S., Ullmann, K., Crounse, J., et al.: Observed NO/NO_2 ratios in the upper troposphere imply errors in NO-NO_2-O3 cycling kinetics or an unaccounted NO_x reservoir, Geophys. Res. Lett, 45, 4466–4474, https://doi.org/10.1029/2018GL077728, 2018.

Stuhlmann, R., Rodriguez, A., Tjemkes, S., Grandell, J., Arriaga, A., Bézy, J.-L., Aminou, D., and Bensi, P.: Plans for EUMETSAT's Third Generation Meteosat geostationary satellite programme, Adv. Space Res, 36, 975–981, https://doi.org/10.1016/j.asr.2005.03.091, 2005.

Tost, H., Jöckel, P., and Lelieveld, J.: Lightning and convection parameterisations – uncertainties in global modelling, Atmos. Chem. Phys., 7, 4568, https://doi.org/10.5194/acp-7-4553-2007, 2007.

van Geffen, J. H. G. M., Eskes, H. J., Boersma, K. F., and Veefkind, J. P.: Report S5P-KNMI-L2-0005-RP, version 2.2.0, released 16 June 2021, KNMI, De Bilt, The Netherlands, https://sentinel.esa.int/documents/247904/2476257/Sentinel-5P-TROPOMI-ATBD-NO2-data-products, 2021.

Veefkind, J., Aben, I., McMullan, K., Förster, H., De Vries, J., Otter, G., Claas, J., Eskes, H., De Haan, J., Kleipool, Q., et al.: TROPOMI on the ESA Sentinel-5 Precursor: A GMES mission for global observations of the atmospheric composition for climate, air quality and ozone layer applications, Remote Sens. Environ., 120, 70–83, https://doi.org/10.1016/j.rse.2011.09.027, 2012.

Vinken, G., Boersma, K., van Donkelaar, A., and Zhang, L.: Constraints on ship NO_x emissions in Europe using GEOS-Chem and OMI satellite NO_2 observations, Atmos. Chem. Phys., 14, 1353–1369, https://doi.org/10.5194/acp-14-1353-2014, 2014.

Wallace, L.: The Spectrum of Lightning., Astrophys. J., 139, 994, 1964.

Wang, P., Stammes, P., der A, R. v., Pinardi, G., and Roozendael, M. v.: FRESCO+: an improved O_2 A-band cloud retrieval algorithm for tropospheric trace gas retrievals, Atmos. Chem. Phys., 8, 6565–6576, https://doi.org/10.5194/acp-8-6565-2008, 2008.

Williams, J. E., Boersma, K. F., Sager, P. L., and Verstraeten, W. W.: The high-resolution version of TM5-MP for optimized satellite retrievals: description and validation, Geosci. Model Dev., 10, 721–750, https://doi.org/10.5194/gmd-10-721-2017, 2017.

Zeldovich, Y., Frank-Kamenetskii, D., and Sadovnikov, P.: Oxidation of nitrogen in combustion, Publishing House of the Acad of Sciences of USSR, 1947.

Zhang, X., Yin, Y., Lapierre, J. L., Chen, Q., Kuang, X., Yan, S., Chen, J., He, C., Shi, R., et al.: Estimates of lightning NO_x production based on high-resolution OMI NO_2 retrievals over the continental US, Atmos. Meas. Tech., 13, 1709–1734, https://doi.org/10.5194/amt-13-1709-2020, 2020.

Zhu, Y., Rakov, V., Tran, M., Stock, M., Heckman, S., Liu, C., Sloop, C., Jordan, D., Uman, M., Caicedo, J., et al.: Evaluation of ENTLN performance characteristics based on the ground truth natural and rocket-triggered lightning data acquired in Florida, J. Geophys. Res. Atmos., 122, 9858–9866, 2017.

Zoogman, P., Liu, X., Suleiman, R., Pennington, W., Flittner, D., Al-Saadi, J., Hilton, B., Nicks, D., Newchurch, M., Carr, J., Janz, S., Andraschko, M., Arola, A., Baker, B., Canova, B., Chan Miller, C., Cohen, R., Davis, J., Dussault, M., Edwards, D., Fishman, J., Ghulam, A., González Abad, G., Grutter, M., Herman, J., Houck, J., Jacob, D., Joiner, J., Kerridge, B., Kim, J., Krotkov, N., Lamsal, L., Li, C., Lindfors, A., Martin, R., McElroy, C., McLinden, C., Natraj, V., Neil, D., Nowlan, C., O'Sullivan, E., Palmer, P., Pierce, R., Pippin, M., Saiz-Lopez, A., Spurr, R., Szykman, J., Torres, O., Veefkind, J., Veihelmann, B., Wang, H., Wang, J., and Chance, K.: Tropospheric emissions: Monitoring of pollution (TEMPO), J. Quant. Spectrosc. Radiat. Transf., 186, 17–39, https://doi.org/10.1016/j.jqsrt.2016.05.008, satellite Remote Sensing and Spectroscopy: Joint ACE-Odin Meeting, October 2015, 2017.

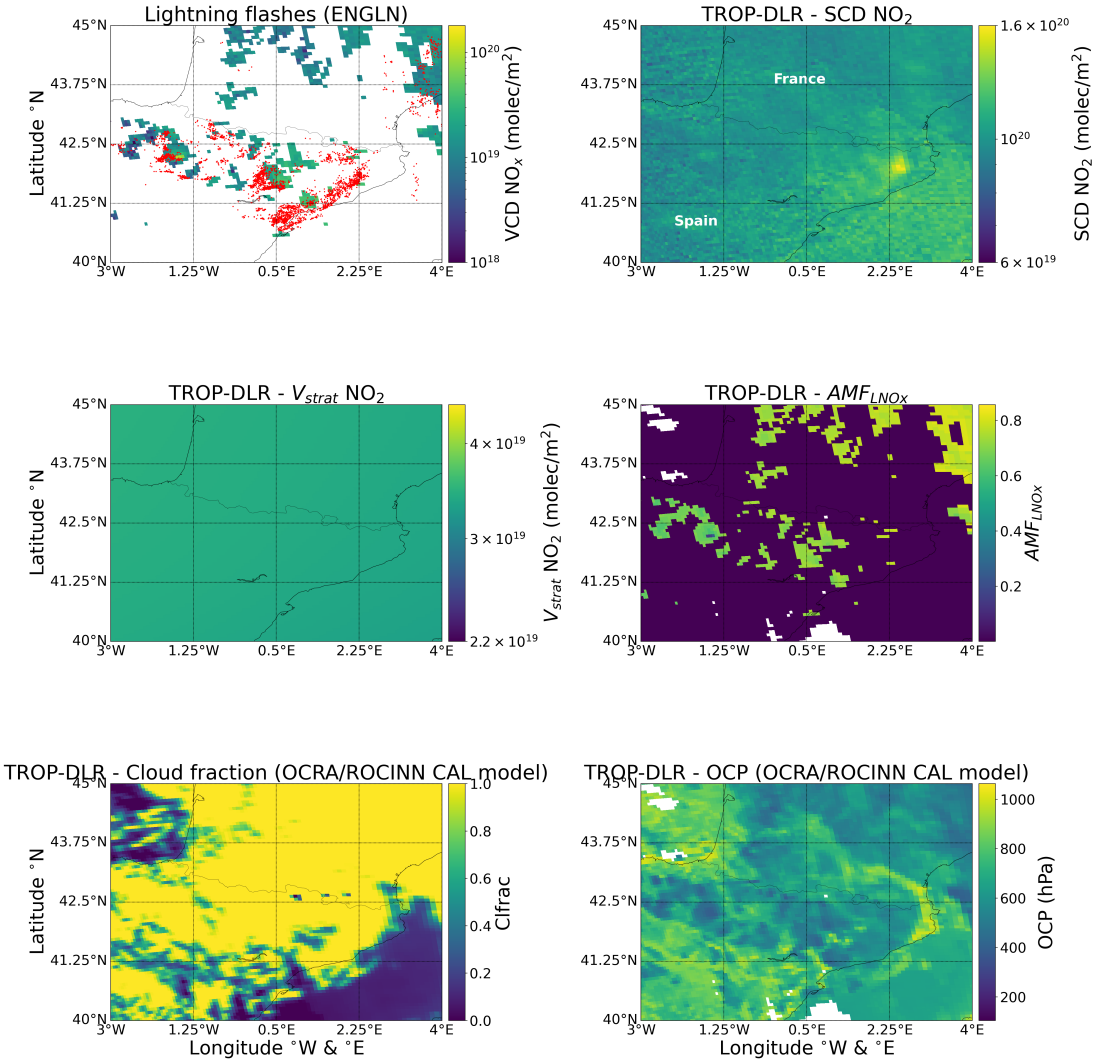

Figure 5. TROP-DLR product and ENGLN lightning data for the case 29 April 2018. The upper left panel shows the positions of lightning flashes (red dots) reported by ENGLN during the 5 h period before the TROPOMI overpass and the calculated VCD NO_x. The upper right panel shows the SCD of NO_2, center left and right panels show the stratospheric VCD ~~and AMF~~ of NO_2 and the AMF_{LNOx}, respectively. The lower left and right panels show the cloud fraction and the OCP, respectively.

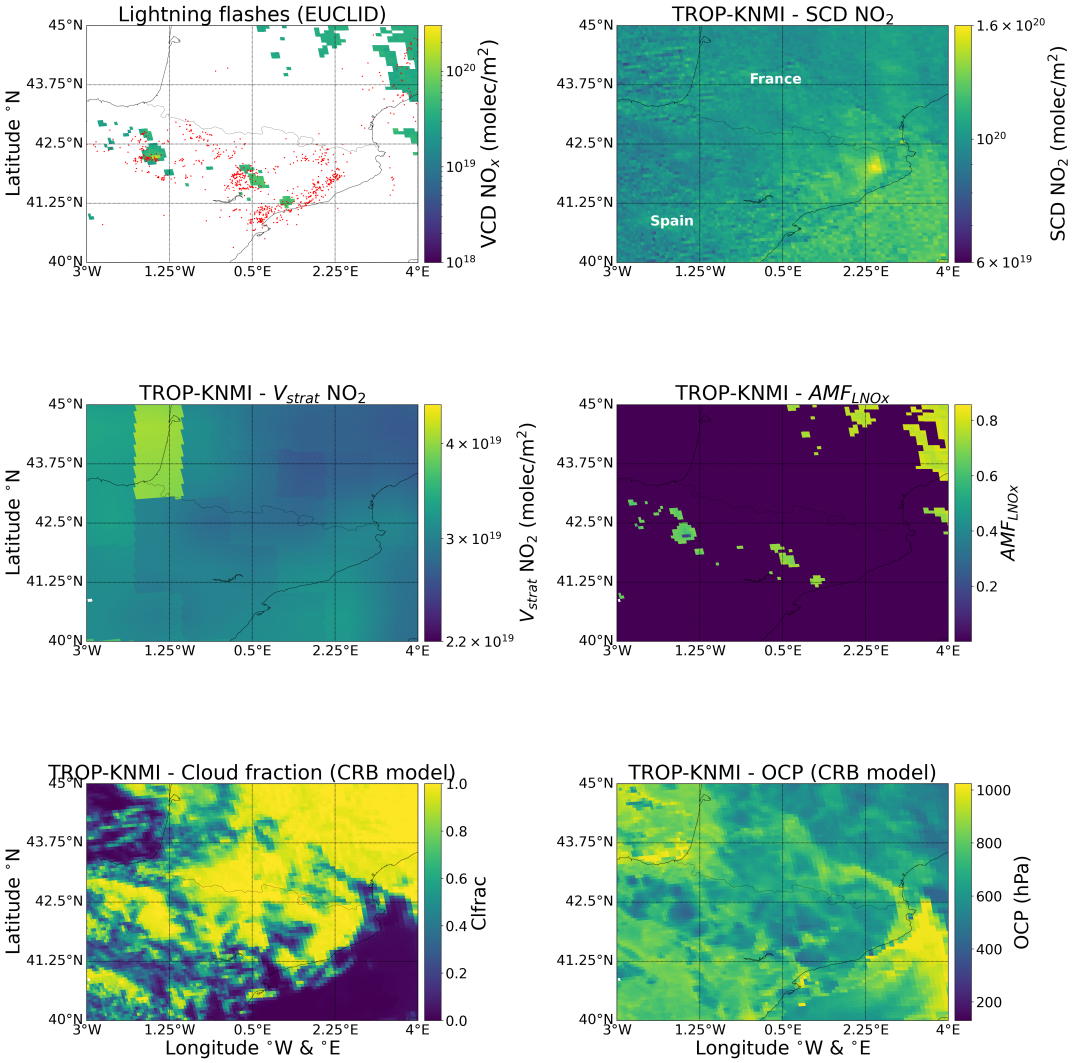

Figure 6. TROP-KNMI product and EUCLID lightning data for the case 29 April 2018. The upper left panel shows the positions of lightning flashes (red dots) reported by EUCLID during the 5 h period before the TROPOMI overpass and the calculated VCD NO_x. The upper right panel shows the SCD of NO_2, center left and right panels show the stratospheric VCD ~~and AMF~~ of NO_2 and the AMF_{LNOx}, respectively. The lower left and right panels show the cloud fraction and the OCP, respectively.

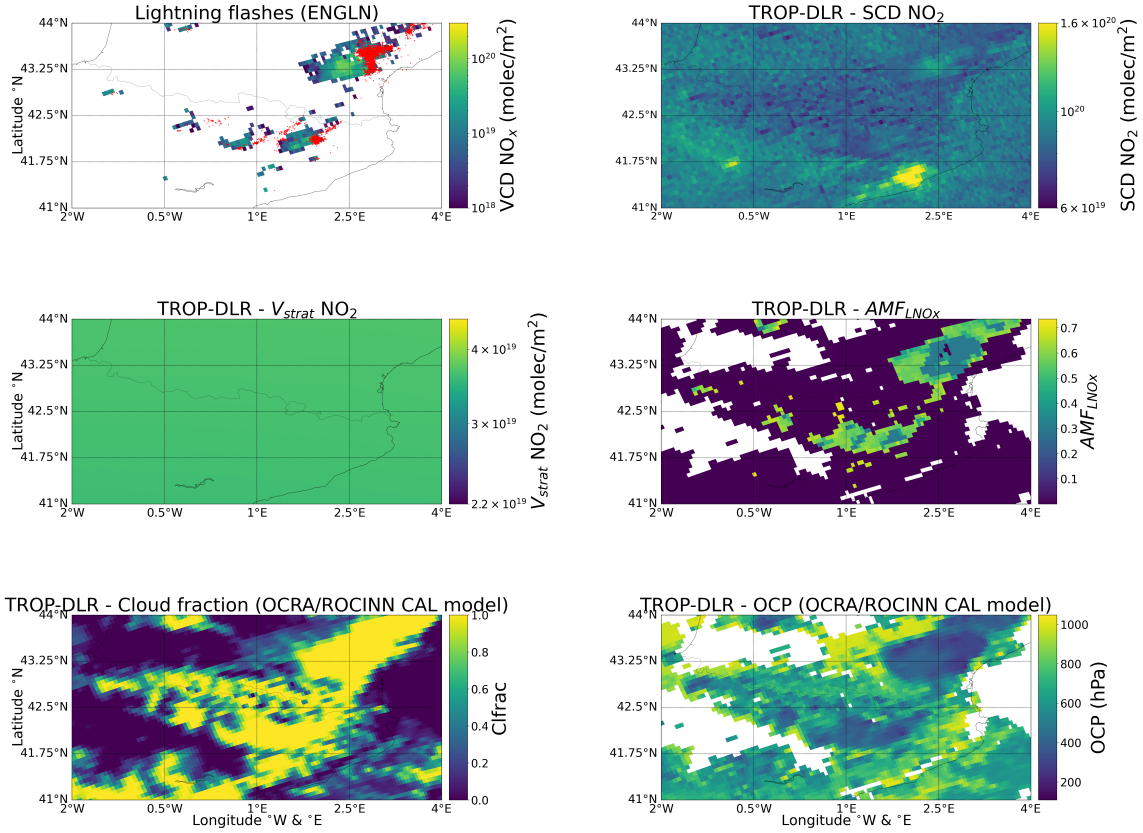

Figure 7. TROP-DLR product and ENGLN lightning data for the case 7 May 2018. The upper left panel shows the positions of lightning flashes (red dots) reported by ENGLN during the 5 h period before the TROPOMI overpass and the calculated VCD NO_x. The upper right panel shows the SCD of NO_2, center left and right panels show the stratospheric VCD ~~and AMF~~ of NO_2 and the AMF_{LNO_x}, respectively. The lower left and right panels show the cloud fraction and the OCP, respectively.

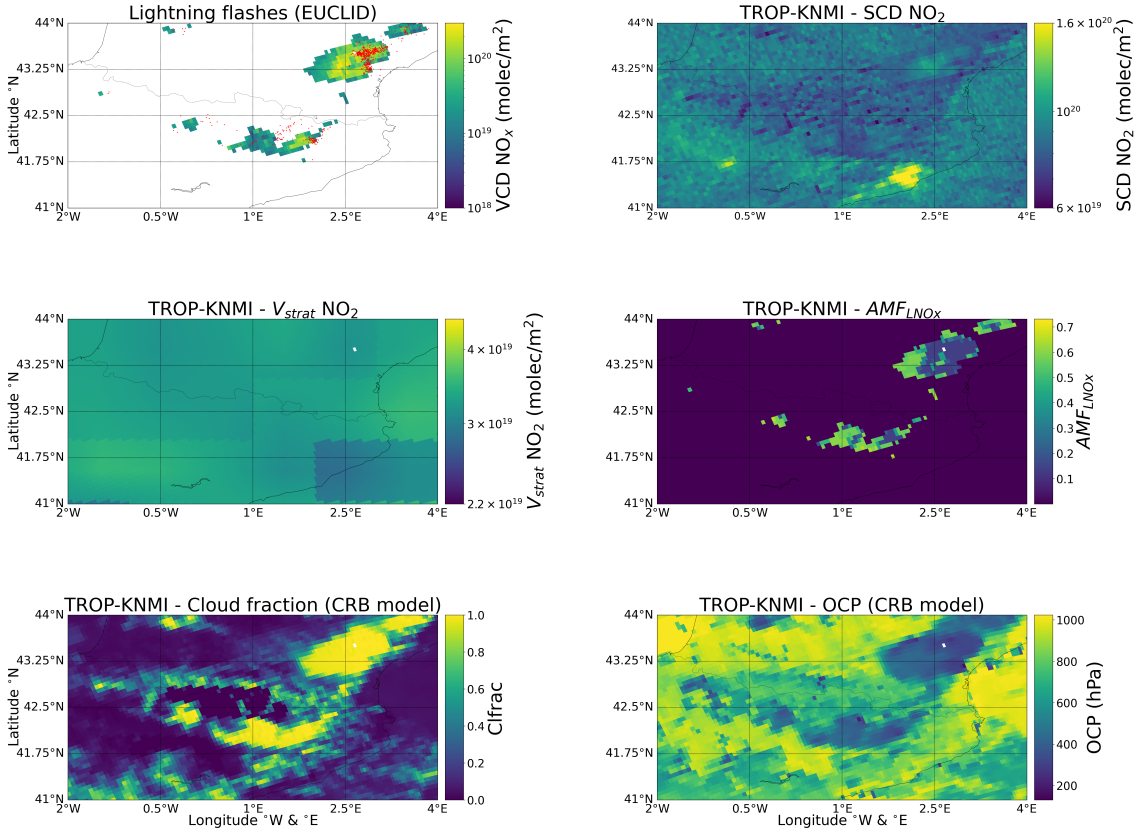

Figure 8. TROP-KNMI product and EUCLID lightning data for the case 7 May 2018. The upper left panel shows the positions of lightning flashes reported by EUCLID (red dots) reported by ENGLN during the 5 h period before the TROPOMI overpass and the calculated VCD NO_x. The upper right panel shows the SCD of NO_2, center left and right panels show the stratospheric VCD ~~and AMF~~ of NO_2 and the AMF_{LNOx}, respectively,. The lower left and right panels show the cloud fraction and the OCP, respectively.

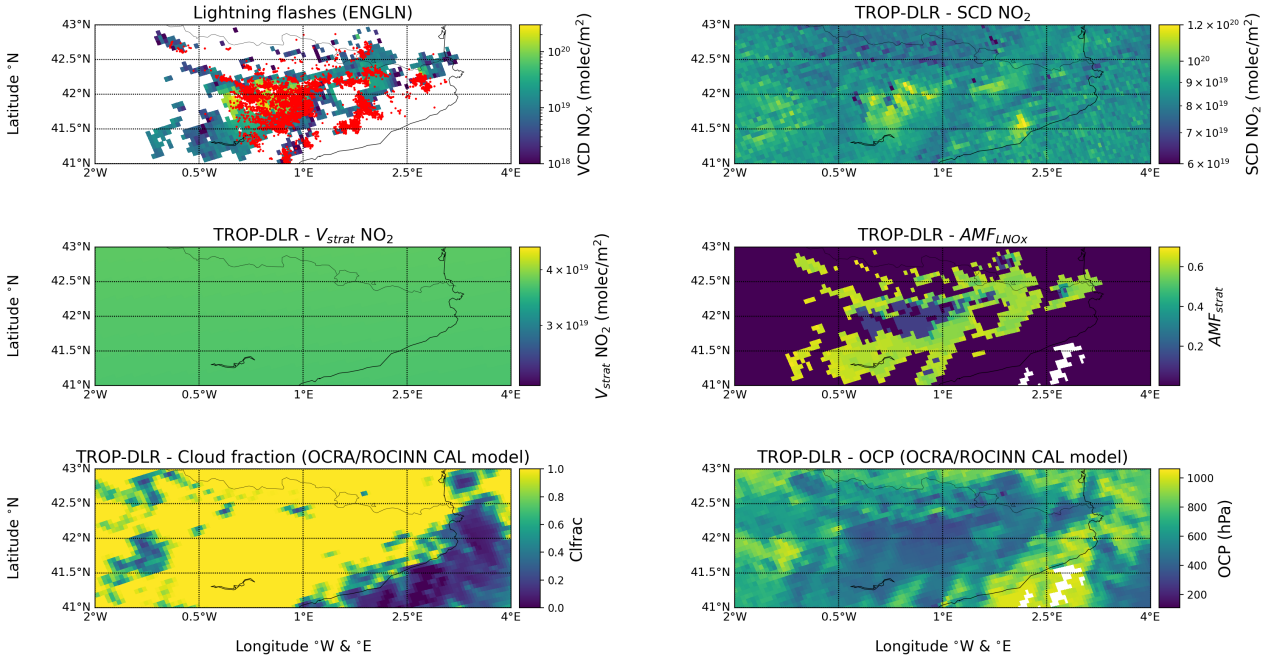

Figure 9. TROP-DLR product and ENGLN lightning data for the case 28 May 2018. The upper left panel shows the positions of lightning flashes (red dots) reported by ENGLN during the 5 h period before the TROPOMI overpass and the calculated VCD NO_x. The upper right panel shows the SCD of NO_2, center left and right panels show the stratospheric VCD ~~and AMF~~ of NO_2 and the AMF_{LNO_x}, respectively. The lower left and right panels show the cloud fraction and the OCP, respectively.

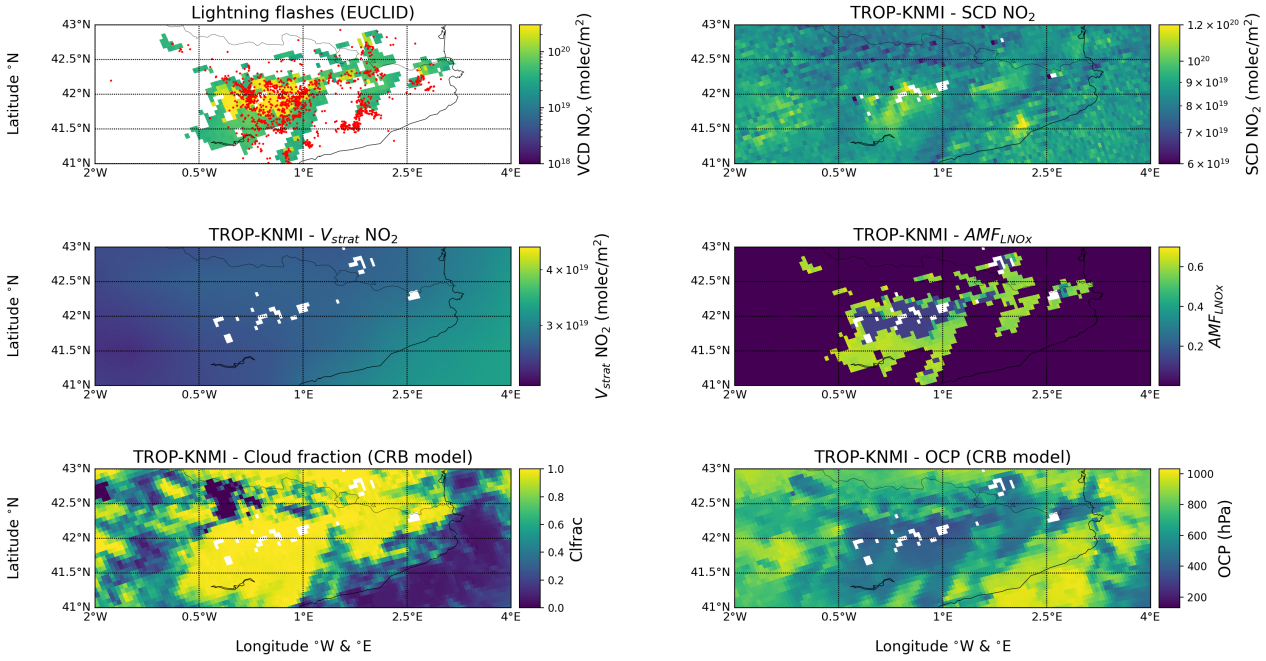

Figure 10. TROP-KNMI product and EUCLID lightning data for the case 28 May 2018. The upper left panel shows the positions of lightning flashes (red dots) reported by EUCLID during the 5 h period before the TROPOMI overpass and the calculated VCD NO_x. The upper right panel shows the SCD of NO_2, center left and right panels show the stratospheric VCD ~~and AMF~~ of NO_2 and the AMF_{LNO_x}, respectively. The lower left and right panels show the cloud fraction and the OCP, respectively.

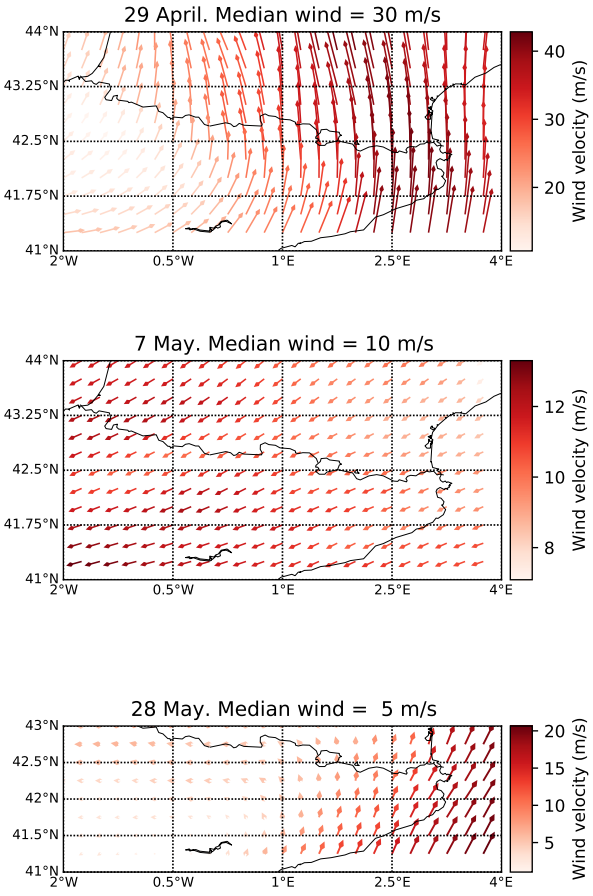

Figure 11. Horizontal wind velocity and direction averaged between 200 hPa and 500 hPa pressure levels for the studied cases on 29 April, 7 May and 28 May, 2018. The horizontal winds are extracted from ERA5-reanalysis data. We show in the title the spatial median of the wind velocity.